THE ASTROPHYSICAL JOURNAL, 615:972–990, 2004 November 10

HEATING PROTOPLANETARY DISK ATMOSPHERES

ALFRED E. GLASSGOLD
Astronomy Department, University of California, 601 Campbell Hall 3411, Berkeley, CA 94720; aglassgold@astron.berkeley.edu

JOAN NAJITA
National Optical Astronomical Observatory, 950 North Cherry Avenue, Tucson, AZ 85719; najita@noao.edu

AND

JAVIER IGEA
Vatican Observatory, Specola Vaticana, V-00120 Vatican City State; jqi6030@planalfa.es
Received 2004 May 7; accepted 2004 July 8

ABSTRACT

We calculate the thermal-chemical structure of the gaseous atmospheres of the inner disks of T Tauri stars, starting from the density and dust temperature distributions derived by D'Alessio and coworkers in 1999. As a result of processes such as X-ray irradiation or mechanical heating of the surface layers, the gas temperature at the very top of the disk atmosphere in the neighborhood of 1 AU is of the order of 5000 K. Deep down, it drops rapidly into the range of the dust temperature, i.e., several hundred degrees kelvin. In between these upper hot and lower cool layers, there is a transition zone with gas temperatures in the range 500–2000 K. The thickness and location of this warm region depend on the strength of the surface heating. This region also manifests the basic chemical transitions of H to H_2 and C^+ and C to CO. It is remarkable that even though the H_2 transition begins first (higher up), it does not go to completion until after CO does. Consequently, there is a reasonably thick layer of warm CO that is predominantly atomic H. This thermal-chemical structure is favorable to the excitation of the fundamental and overtone bands of CO because of the large rate coefficients for vibrational excitation in H+CO as opposed to H_2+CO collisions. This conclusion is supported by the recent observations of the fundamental band transitions in most T Tauri stars. We also argue that layered atmospheres of inner T Tauri disks may play an important role in understanding the observations of H_2 UV fluorescence pumped from excited vibrational levels of that molecule. Possible candidates for surface heating include the interaction of a wind with the upper layers of the disk and dissipation of hydromagnetic waves generated by mechanical disturbances close to the midplane, e.g., by the Balbus-Hawley instability. Detailed modeling of the observations has the potential to reveal the nature of the mechanical surface heating that we model phenomenologically in these calculations and to help explain the nature of the gas in protoplanetary disks.

Subject heading: planetary systems: protoplanetary disks

1. INTRODUCTION

Disks surrounding solar mass stars at ages less than a few million years appear to be young analogs of our solar system and thus systems in which the formation of planetary systems may be underway. They are therefore useful laboratories in which to study the processes involved in the formation of stars and planets. Observations of disks may provide insight into the processes responsible for angular momentum transport in disks. They may also probe the timescales for grain growth and gas dissipation, measurements needed to explore the likelihood of planetary systems like our own. The inner regions of disks ($\lesssim$10 AU) are of particular interest in this regard. Both terrestrial and giant planets are believed to form in this region. In addition, the large number of extrasolar giant planets that are found at small orbital radii, within a few AU of their central stars, suggests that giant planets migrate frequently through the inner disk (e.g., Bodenheimer & Lin 2002).

Since the angular scale subtended by the inner disk at the distance of the nearest nearby star-forming region is currently beyond our ability to spatially resolve, it is particularly important to develop gas-phase diagnostics of this region. With velocity-resolved observations of these diagnostics, disk radii can be separated in velocity in order to recover the structure of the disk. Gas-phase diagnostics are also valuable because they can measure gas column densities and masses, gas temperatures, and the chemical abundance structure of the gaseous disk. Observational constraints on these quantities may provide new insights into the physical processes that govern planet formation. For example, the measurement of gas masses in the inner disk may constrain the gas dissipation timescale, and thereby the time available for giant planet formation. Studies of the gaseous component in disks are also relevant to the possibility of forming solar systems like our own. For example, residual gas in the terrestrial planet region of the disk may play an important role in determining the ultimate mass and eccentricity of a terrestrial planet and its consequent habitability (e.g., Kominami & Ida 2002).

Although primordial (unevolved) planet-forming disks are expected to be very optically thick (e.g., at 1 AU the column density of the minimum-mass solar nebula is $\sim$1500 g cm^{-2}), emission lines are nevertheless expected from disks in several situations. Since disks are externally irradiated (e.g., by the central star), the gaseous component of disks may be detectable through emission lines produced in temperature inversion regions of the disk atmosphere, i.e., in disk "chromospheres." Line emission may also arise from regions of low continuum opacity produced, e.g., through grain growth and planetesimal formation. Line emission also may arise from regions of intrinsically low column density that are produced through disk dissipation (e.g., the accretion of the disk onto the star). Low column density regions may also result from the presence of stellar or planetary companions, which can sculpt the disk and reduce the disk column density in the vicinity of the companion's orbit.

Indeed, there now exist multiple gas-phase probes of the inner disk region. These include the fundamental and overtone transitions of CO (e.g., Najita et al. 2003; Carr et al. 1993), infrared rovibrational transitions of water (Carr et al. 2004), and UV transitions of H_2 (e.g., Herczeg et al. 2002). These diagnostics have been used to illustrate the differential rotation of disks (e.g., Carr et al. 2004; Najita et al. 2000; see also Hartmann & Kenyon 1987a, 1987b in the context of FU Orionis stars), the existence of suprathermal line broadening possibly produced by turbulence in disks (Carr et al. 2004; Najita et al. 1996), the existence of residual gas in disk gaps (Carr et al. 2001), significant departures from chemical equilibrium in the relative abundance of water and CO in the inner disk (Carr et al. 2004), and the presence of surprisingly warm gas ($\sim$1000 K) in the terrestrial planet regions of disks (Najita et al. 2003; Herczeg et al. 2002).

The interpretation of these diagnostics requires models of gaseous disk atmospheres in the inner disk region. For example, the conversion of measured column densities of a given species (e.g., CO or H_2) to total mass column density requires a model of the thermal, chemical, and excitation structure of the atmosphere. Including the chemistry of the atmosphere is important for determining the temperature because atoms and molecules, as emitters (or absorbers) of line radiation, cool (or heat) the gas. Atoms and molecules also provide diagnostic lines that can be used to determine the physical properties of the gas. For example, measurements of relative abundances, intrinsic line widths, and the strengths of individual emission lines can be analyzed using models of gaseous atmospheres to diagnose the vertical thermal, chemical, and turbulent structure of the atmosphere. The deduced structure may, in turn, reveal the heating and related dynamical processes that operate in the atmosphere.

Recent studies have begun to investigate the role of Lyα photons in the surface excitation of the inner disk (Herczeg et al. 2002, 2004), as well as in the chemistry of the outer disk (Bergin et al. 2003). However, most studies of the thermal structure of disk atmospheres to date have focused on the properties of the dust component of the atmosphere (e.g., Chiang & Goldreich 1997; D'Alessio et al. 1998, 1999, 2001; Calvet et al. 1991; Dullemond et al. 2002). In these models, the dust temperature is determined by the absorption of stellar photons and the reemission of the absorbed energy. The models of D'Alessio et al. (1998, 1999, 2001) formally include the gaseous component of the atmosphere as a opacity source, but because the dust dominates the opacity for both absorption and emission and the gas and dust are assumed to be thermally coupled, the calculation is strongly weighted toward the dust component. Indeed, the thermal structure produced by these calculations provides a good description of the dust spectral energy distributions of T Tauri stars.

The assumption that the gas and dust components have the same temperature is common in the literature, but clearly, as pointed out by Chiang & Goldreich (1997), this must break down at some height in the atmosphere where the density is too low to ensure good thermal coupling. The density at which the dust becomes decoupled from the gas can be estimated by comparing the collisional timescale, $\tau_g = 1/n_{\rm H}\bar{v}\pi a^2$ (where a is the radius of a dust grain and $\bar{v}$ is the mean speed of a gas atom or molecule), with other thermal timescales. For example, the time for a dust particle of radius a and temperature $T_d(a)$ to radiate, $kT_d/4\pi a^2\sigma_{\rm SB}T_d^4$, is shorter than the collisional timescale unless the gas density is larger than a critical density (see also Chiang & Goldreich 1997),

$$n_{\rm cr} = \frac{4\sigma_{\rm SB}T_d^3}{k\bar{v}} = \left(1.133\times10^8\ {\rm cm}^{-3}\right)\frac{T_d^3}{T_g^{1/2}}, \qquad (1)$$

assuming that the gas is molecular hydrogen. Consequently, in a warm disk atmosphere at radial distances $\sim$1 AU, $n_{\rm cr} \sim 10^{13}$–10^{14} cm^{-3}, and the dust is uncoupled from the gas above several midplane scale heights. Determining the region in which the gas becomes decoupled from the dust (i.e., where gas-dust collisions do not play a significant role in determining the gas temperature) is more difficult to estimate and is one of the goals of this paper.

When the thermal coupling of the gas to the dust is weakened, e.g., as a consequence of the low density in the upper atmosphere, the gas temperature is no longer strictly regulated by the dust. The gas may be at a higher or lower temperature than the dust, depending on the strength of the heating and cooling processes. We have previously commented that stellar X-rays may be significant in heating gaseous disk atmospheres because young stars are known to be strong X-ray emitters (e.g., Feigelson & Montmerle 1999). In a preliminary study, we found that X-ray heating can induce an inversion in the gas temperature distribution over a column density comparable to that in which the dust experiences a temperature inversion (Glassgold & Najita 2001). The gas temperature ($\sim$1000 K) may actually exceed the dust temperature ($\lesssim$400 K at 1 AU; D'Alessio et al. 1999, 2001) in the region of the inversion. This preliminary work showed that the dust and gas at moderately high altitudes behave as two separate but weakly coupled thermodynamic systems. In addition to the weak collisional interaction discussed above, the dust and gas differ markedly in their radiative properties. Unlike the dust, the gas absorbs very little of the stellar optical-infrared radiation. It has to depend on the relatively small fraction of the star's luminosity that emerges at X-ray wavelengths, $L_{\rm X}/L \sim 10^{-4}$ to 10^{-3}, for any stellar heating. Similarly, line cooling by atoms and molecules is weaker than the continuum radiation emitted by the dust. The much smaller wavelength region over which the gas is radiatively heated and cooled, compared to the dust, suggests that gas-grain collisions play a much larger role in determining the gas temperature than they do for the dust temperature.

Thus, calculating the gas temperature in the atmosphere of the inner disk requires a reasonably complete treatment of heating and cooling processes. In this paper we expand on Glassgold & Najita (2001) and carry out a more detailed, but still approximate, study of the thermal and chemical structure of the gaseous atmosphere. In addition to X-ray heating of the gas, we include the effects of accretion-related heating processes in the atmosphere. We also consider how grain growth affects the thermal coupling of the gas and dust.

Grain growth and settling both act to diminish the coupling between the gas and dust through reductions in the mean grain cross section per unit grain mass and in the dust-to-gas ratio. Indeed, grain growth appears to be a significant effect in the outer regions of T Tauri disks, as suggested by the models of D'Alessio et al. (1998, 1999, 2001; see also Miyake & Nakagawa 1993; Wood et al. 2001). For example, D'Alessio et al. (1999) argue that, if T Tauri disks are filled with small grains like those in the interstellar medium (ISM), the resulting disk scale height is too large to be consistent with several observational constraints. As a result of their dramatic flaring, disks with ISM grains would extinct too much of the stellar light; they would also produce an excess of flux in the 25–100 μm region. Furthermore, when viewed in scattered light, disks would also appear to be more extended than observed.

D'Alessio et al. (2001) have interpreted these difficulties as evidence for grain growth. With a grain size distribution that extends to larger grains ($\sim$1 mm), there is less projected grain surface area and, as a result, the opacity to stellar photons is reduced. Stellar photons therefore penetrate further and produce a temperature inversion deeper down in the atmosphere. In addition, larger grains emit more efficiently at the long wavelengths at which the absorbed radiation is reemitted. As a result of both of these considerations, the disk atmosphere has a correspondingly smaller scale height, in better agreement with observations. Since grain growth is thought to occur as a consequence of grain settling (Weidenschilling 1997), it seems reasonable to assume that grain settling has also occurred in T Tauri disks.

Although the grain growth and settling deduced from disk spectral energy distributions apply more directly to the outer disk, simple estimates suggest that grain settling is even more rapid at smaller radial distances. For example, the settling speed of a grain of radius a and internal density $\tilde{\rho}$ at a height z above the disk midplane is $v_z \simeq \Omega^2 \tilde{\rho} a z / \rho_g c$, where Ω is the disk angular rotation speed, ρ_g is the gas density, and c is the sound speed (Goldreich & Ward 1973). For a disk surrounding a 1 $M_\odot$ star that has a constant temperature of 400 K at 1 AU, a total vertical column density of 1500 g cm^{-2} (as in the minimum-mass solar nebula), and is filled with grains with an internal density $\tilde{\rho} = 1$ g cm^{-3}, the time for grains to settle from the upper disk atmosphere down to a height $z/H = 2.0$ is $\sim$3000 yr for 1 μm grains and $\sim$30,000 yr for 0.1 μm grains. In settling, the grain travels through a column density of $\sim 10^{24}$ cm^{-2} or $\sim$2 g cm^{-2}. Therefore, on a timescale much shorter than the age of T Tauri stars, even micron-sized grains may become depleted from the upper disk atmosphere if there is no mixing of the settling grains back into the upper atmosphere. Turbulence in the midplane, induced as part of the accretion process, is one possible mixing process. However, simulations of grain growth and settling in a turbulent disk (Weidenschilling & Cuzzi 1993) also find that grains settle rapidly out of the upper atmosphere, with a reduction in grain abundance of $>10^3$ on timescales of 10^4 yr. If grains are consequently depleted from the upper disk atmosphere as a result of settling, the lower grain abundance will reduce the efficiency of gas-grain collisions in heating or cooling the gas, with a consequent effect on the disk atmospheric structure. It will also reduce the contribution of grain surface reactions to molecule formation.

We consider both of these effects in the calculations presented here. We assume a reduced mean grain cross section in order to explore the effect of grain growth on the thermal structure of the gaseous atmosphere, and molecule formation on grains is not included in the chemical network. The lower gas-grain collision rate that results from the reduced grain cross section can also result from grain settling, although this effect, a reduction in the total mass of grains at a given vertical height, is not included explicitly in the calculation. We also explore the effect of accretion-related processes (e.g., possible viscous accretion in the disk atmosphere and energy dissipation in a wind-disk mixing layer) on the thermal-chemical structure of the gaseous disk atmosphere. We specifically focus on the region of the disk at 1 AU in order to address the disk spectroscopic results described above.

Since our goal at this stage is to illustrate the general character of the gaseous atmosphere of the inner disk rather than to make detailed predictions, we have taken the liberty of greatly simplifying the calculation. We assume that the density structure and dust temperature structure of the atmosphere are as given in the T Tauri disk model of D'Alessio et al. (1999), and we calculate the gas temperature and chemical structure that would exist under those conditions. A serious limitation of our calculation is that the gas temperature and density structure are not calculated self-consistently. A more complete calculation would begin with a two-fluid model for the gas and dust, with the gas in hydrostatic equilibrium and the dust suspended to the extent allowed by grain growth and settling. We discuss the impact of this limitation in § 6.

In § 2 we discuss the heating and cooling processes that affect the thermal structure of the gaseous atmosphere. Many of the technical details are contained in a series of appendices. A description of the chemistry that takes place within this thermal structure is presented in § 3. The resulting thermal-chemical structure of the atmosphere is discussed in § 4. In § 5 we discuss these results in the context of recent observations of gas-phase diagnostics of inner disks. Finally, in § 6 we summarize our results and discuss possible future directions for these studies.

2. THERMAL STRUCTURE OF THE ATMOSPHERE

In studying the thermal structure of gaseous disk atmospheres, as is often the case in other astrophysical contexts, identifying the gas-heating agents is more difficult than identifying the cooling agents. We consider several viable heating processes: dust-gas collisions, X-rays, accretion viscosity, and the interaction of the wind with the disk. Dust-gas collisional heating (or cooling) in the ISM is well known (e.g., Spitzer 1949; Goldreich & Kwan 1974; Hollenbach & McKee 1979; Takahashi et al. 1983), and here we add an explicit treatment of its dependence on the size distribution of the dust grains. Our consideration of X-ray heating is a natural extension of previous work on X-ray ionization of disks (Glassgold et al. 1997, hereafter G97; Igea & Glassgold 1999, hereafter IG99). The potentials of both accretion and wind-disk heating were suggested even earlier by our collaborators and us in connection with the gas temperature inversion observed in Herbig Ae/Be stars (Carr et al. 1993; Najita et al. 1996) but not investigated in any detail.

2.1. *Dust-Gas Heating and Cooling*

Dust warmed by radiation from the central star can heat the gas by collisions if the dust is hotter than the gas, a situation often encountered for interstellar clouds. Because of weak gas cooling in disks, we are more concerned with the situation where the gas is hotter than the dust and the collisions cool the gas. Since the drift velocity is much smaller than the sound speed, we can adapt the standard interstellar formula in Hollenbach & McKee (1979) to obtain the cooling rate per unit volume by spherical grains in a mixture of atomic and molecular hydrogen,

$$\Lambda_{dg} = \mathcal{A}_{\rm H} n_d(a) n_{\rm H} \bar{v}({\rm H}) 2k \left[T_g - T_d(a)\right] \pi a^2, \qquad (2)$$

where $n_d(a)$ is the volume density of the grains of radius a with mean temperature $T_d(a)$, $n_{\rm H}$ is the volume density of hydrogen nuclei, and $\bar{v}(\mathrm{H})$ is the mean speed of a hydrogen atom. The mean accommodation coefficient $\mathcal{A}_{\mathrm{H}}$ can be obtained from the estimates of Burke & Hollenbach (1983) for atomic and molecular hydrogen,

$$\mathcal{A}_{\mathrm{H}} = x(\mathrm{H})\mathcal{A}(\mathrm{H}) + \frac{1}{\sqrt{2}} x(\mathrm{H}_2)\mathcal{A}(\mathrm{H}_2), \tag{3}$$

where $\mathcal{A}(\mathrm{H})$ and $\mathcal{A}(\mathrm{H}_2)$ are the accommodation coefficients for atomic and molecular hydrogen, respectively, and the $1/\sqrt{2}$ factor corrects for the mean speed of H_2. The abundances of atomic and molecular hydrogen, as well as all other abundances in this paper, are normalized to the total density of hydrogen nuclei n_{H}, i.e., $x(\mathrm{H}) = n(\mathrm{H})/n_{\mathrm{H}}$, $x(\mathrm{H}_2) = n(\mathrm{H}_2)/n_{\mathrm{H}}$, and $x(\mathrm{H}) + 2x(\mathrm{H}_2) = 1$. Equation (2) ignores He collisions and the correction $2kT_g \rightarrow 2kT_g + E_{\mathrm{int}}$ for the internal excitation energy E_{int} of H_2. The mean temperature of a grain of radius a is obtained by balancing absorption and emission, assuming that the absorption occurs at high frequency, where the absorption coefficient $Q_\nu \simeq 1$, and that the emission occurs at low frequencies, where $Q_\nu \propto \nu^\beta$. In this case,

$$T_d(a) \propto a^{-b}, \quad b = \frac{\beta}{4+\beta}, \tag{4}$$

and $T_d(a)$ varies as a small inverse power, $b = \frac{1}{5}-\frac{1}{3}$, when the index of the absorption coefficient $\beta \simeq 1$–2.

In Appendix A we average equation (2) over the MRN dust-size distribution (Mathis et al. 1977), $n_d(a) = C_p a^{-p}$ ($a_1 < a < a_2$). We find that, for $p = 3.5$,

$$\Lambda_{dg} = \frac{\rho_d}{(4\pi/3)\tilde{\rho} a_g^3} n_{\mathrm{H}} \bar{v}(\mathrm{H}) 2\mathcal{A}_{\mathrm{H}} k \left(T_g - \bar{T}_d\right) \pi a_g^2, \tag{5}$$

where ρ_d is the volumetric mass density of dust in the disk, $\tilde{\rho}$ is the internal density of a dust grain, assumed to be independent of size, $a_g = (a_1 a_2)^{1/2}$, and $\bar{T}_d$ is the grain area-weighted average of $T_d(a)$. As shown in Appendix A, $\bar{T}_d$ differs from the simple unweighted average by a factor B (defined in eq. [A7]) that is somewhat smaller than unity for grain distributions with $a_2/a_1 \gg 1$ and slightly greater than unity for a_2 comparable with a_1. This factor arises because the second term of equation (2) leads to the $(2 - b)$-moment of the MRN distribution and emphasizes slightly smaller (and warmer) grains than the first. In this paper we assume that the area-weighted average dust temperature $\bar{T}_d$ (as well as the hydrogen gas density n_{H}) is the same as the temperature calculated by D'Alessio et al. (1999). The most important consequence of averaging over grain size is that the cooling rate equation (5) is inversely proportional to the geometric mean of the minimum and maximum grain sizes.

A numerical version of equation (5) is

$$\Lambda_{dg} = \left(2.38\times10^{-33} \text{ ergs cm}^3 \text{ s}^{-1} \text{ K}^{-3/2}\right)\left(\frac{\rho_d}{\rho_g}\right)_{0.01} \times \left(\frac{0.05\ \mu\mathrm{m}}{a_g}\right)\left(\frac{\mathcal{A}_{\mathrm{H}}}{0.5}\right) T_g^{1/2}\left(T_g - \bar{T}_d\right) n_{\mathrm{H}}^2, \tag{6}$$

where the dust-to-gas ratio is ratioed to 0.01 and the accommodation coefficient to 0.5. The MRN grain size distribution has $a_1 = 0.005$ μm and $a_2 = 0.25$ μm, or $a_g = 0.035$ μm. However, there is good evidence for grain evolution in both dense regions of the ISM (e.g., Kim et al. 1994) and T Tauri disks (D'Alessio et al. 2001; Wood et al. 2001; Wolf et al. 2003; McCabe et al. 2003). Adopting the parameters used by Wood et al. (2001), which correspond to $a_1 = 0.01$ μm, $a_2 = 50$ μm, and $a_g = 0.707$ μm, leads to an increase in the geometric mean grain size by a factor of about 20, with a corresponding decrease in dust-gas cooling. If we were to use the grain model in D'Alessio et al. (2001), which produces a good fit to the millimeter-wave portion of T Tauri spectral energy distributions, then $a_g = 7.07$ μm, and dust-gas cooling would be reduced by another order of magnitude. Inclusion of the effects of dust settling, in addition to grain growth, would further reduce our numerical estimate of this rate (through the proportionality to the dust-to-gas ratio), whereas any form of preferential gas loss would have the opposite effect.

2.2. *X-Ray Heating*

X-rays incident on the disk produce fast electrons that heat the gas, as discussed by G97 for T Tauri disks and by Shang et al. (2002) for T Tauri winds. The heating rate is given by

$$\Gamma_{\mathrm{X}} = \zeta_{\mathrm{X}} \Delta\epsilon_h n_{\mathrm{H}}, \tag{7}$$

where ζ_{X} is the total ionization rate and $\Delta\epsilon_h$ is the heating rate per ionization. We follow Shang et al. (2002) in adapting the treatment of the heating rate by Shull & van Steenberg (1985) but extend it to H_2 regions using the more general results of Dalgarno et al. (1999). Shang et al. (2002) found that, in addition to the usual direct X-ray heating energy $\Delta\epsilon_{h1}$ (in the range 5–15 eV), there is an indirect heating energy $\Delta\epsilon_{h2}$ that arises from the increase in the population of electronically excited states produced by X-rays and leads to gas heating by collisional de-excitation. The indirect heating energy for atomic H is 23 eV, and we expect the same order of magnitude for H_2. Thus, we express the total X-ray heating as

$$\Delta\epsilon_h = \Delta\epsilon_{h1} + \Delta\epsilon_{h2}, \tag{8}$$

with $\Delta\epsilon_{h1} \sim 10$ eV and $\Delta\epsilon_{h2} \sim 20$ eV.

In order to calculate the total ionization rate, we need the individual rates for ionizing H, He, and H_2, which are also essential for the chemistry. The production rate for ion X^+ at a radial distance r from the star is approximately given by

$$\zeta(\mathrm{X}^+) = \frac{1}{4\pi r^2} \int_{E_0}^{\infty} dE\, L(E) e^{-N_{\mathrm{H}}\sigma(E)} \frac{1}{W(\mathrm{X}^+)}, \tag{9}$$

where $L(E)$ is the spectral distribution of the X-ray luminosity and $W(\mathrm{X}^+)$ is the mean energy to make an ion X^+; $\zeta(\mathrm{X}^+)$ is defined so that the ionization rate per unit volume is $\zeta(\mathrm{X}^+)n_{\mathrm{H}}$. The exponential factor gives the attenuation along the line of sight to the location r, and N_{H} is the hydrogen column density along this line of sight. The X-rays generally penetrate the disk at fairly small angles, so that the disk is not irradiated directly from above but at low inclination.[1] The X-ray absorption cross section σ is taken from Morrison & McCammon (1983). For $E \gg 0.1$ keV, we may approximate $\mathcal{A}_{\mathrm{el}}$ and the $W(\mathrm{X}^+)$ by constants and use $W(\mathrm{H}^+) \approx 40$ eV, $W(\mathrm{H}_2^+) \approx 40$ eV, and $W(\mathrm{He}^+) \approx 475$ eV for the mean energies to produce H^+, H_2^+,

[1] The line-of-sight column density N_{H} in eq. (9) is much larger than the vertical column density $N_\perp$ introduced in eq. (19) of § 3. The latter quantity is provided as a useful alternative z-coordinate.

and He^+ ions (Dalgarno et al. 1999).[2] The result is that the ionization rates for these ions are

$$\zeta(H^+) = \zeta_0 x(H), \quad \zeta(H_2^+) = \zeta_0 2x(H_2),$$
$$\zeta(He^+) = 0.082\zeta_0 \sim \zeta_0 x(He), \tag{10}$$

where ζ_0 is the rate at which H^+ ions are produced per hydrogen atom using $W(H^+) = 40$ eV. Defining ζ_X so that $\zeta_X n_H$ is the X-ray ionization rate per unit volume in an H, H_2, He mixture, the sum of the terms in equation (10) leads to $\zeta_X = 1.084\zeta_0$ or, if we ignore the difference between 0.082 and $x_{He} = 0.1$,

$$\zeta_X \simeq (1 + x_{He})\zeta_0. \tag{11}$$

Following previous work (G97; IG99), we use a thermal X-ray spectral distribution with $L_X = 2\times10^{30}$ ergs s^{-1}, $kT_X = 1$ keV, and a low-energy cutoff $E_0 = 0.1$ keV. Our choice of L_X is suggested by the average YSO X-ray luminosity found with *Chandra* for stellar masses in the 0.8–1.2 $M_\odot$ range for the Orion Nebula Cloud (Garmire et al. 2000). A slightly smaller L_X has been obtained for YSOs older than 1 Myr, but in a broader range of stellar masses, 0.7–1.4 $M_\odot$ (Feigelson et al. 2002). This choice also applies to TW Hydrae, the nearest classical T Tauri star (Kastner & Weintraub 2002). With the adopted YSO X-ray parameters, the ionization rate at the top of the disk atmosphere at a radial distance of 1 AU is $\zeta_X \simeq 6\times10^{-9}$ s^{-1}.

2.3. *Accretion Heating*

Viscous accretion, driven, for example, by the widely favored Balbus-Hawley magnetorotational instability (MRI; Stone et al. 2000), may also result in the heating of disk surface layers. This can occur if the surface layers are the only regions of the disk sufficiently ionized to participate in the MRI at small radii (Gammie 1996; G97; Fromang et al. 2002). Alternatively, accretion in the disk midplane may generate waves that propagate into the disk atmosphere, steepen into shocks, and dissipate energy there (Miller & Stone 2000). We are led to approximate these effects by adapting the standard dissipation rate for a thin disk (Pringle 1981),

$$\Gamma_{acc} = \tfrac{9}{4}\alpha_h \rho c^2 \Omega, \tag{12}$$

where ρ is the local mass density, c is the isothermal sound speed, and Ω is the angular rotation speed. We regard α_h as a phenomenological parameter that specifies the magnitude of the heating rate. D'Alessio et al. (1998, 1999, 2001) use this formula in calculating the vertical thermal structure of flared disks but with $\alpha_h = \alpha$, the standard α-disk parameter that relates viscous heating to an accretion rate.

In applying the phenomenological formula, equation (12), to surface layers, we need to ask what would be an appropriate value for α_h for these regions. D'Alessio et al. (1998, 1999, 2001) have usually chosen $\alpha = 0.01$ on the basis of the connection between α and the disk accretion rate: $\dot{M}_D \propto \alpha\Sigma_D$, where Σ_D is the integrated disk surface density. According to α-disk theory, this familiar relation applies to the bulk of the accreted material that is located close to the midplane. In the present application, we apply equation (12) to a thin surface region that amounts to less than 1% of the total surface density of the disk. We would argue that α_h varies with position in a truly three-dimensional disk, depending on the details of the accretional dissipation process. For example, α_h may be larger in surface regions if they carry a significant fraction of the mass flux, as implied by MRI layered accretion.[3] Other heating processes may provide enhanced surface heating, e.g., magnetic reconnection and gravitational instabilities operate primarily near the midplane but can transmit energy to the surface by waves. The prescription in equation (12) might also represent the energy dissipation that occurs where the wind interacts with the surface of the disk, a process discussed in the next section. Basically, however, in the absence of a fundamental theory, we adopt the view that the α_h in our "accretion heating" formula should be determined by observations that are sensitive to the thermal properties of disk surface layers. In § 4 we arrive at some preliminary conclusions based on this approach.

Equation (12) can be put into a useful form for numerical evaluation,

$$\Gamma_{acc} = \gamma_{acc} n_H, \quad \gamma_{acc} \equiv \frac{9}{4} 1.425 \alpha_h m_H c^2 \Omega, \tag{13}$$

using $1.425m_H$ as the mass per H nucleus. Since $mc^2 = kT_g$, we evaluate γ_{acc} as

$$\gamma_{acc} = \left(8.82\times10^{-23}\ \text{ergs s}^{-1}\ \text{K}^{-1}\right)\left(\frac{m_H}{m}\right)\alpha_h T_g \left(\frac{\text{AU}}{\varpi}\right)^{3/2}, \tag{14}$$

where ϖ is the radial cylindrical coordinate.

2.4. *Wind-Disk Heating*

Winds generated close to the star, perhaps near the inner edge of the disk, as in an *X*-wind, will blow over the disk and produce a turbulent mixing layer that results in heating of disk surface layers (called an "aeolosphere" by Carr et al. 1993). Although this layer has been discussed before in the context of disk dissipation by Elmegreen (1978) and more recently by Hollenbach et al. (2000), its thermal properties have not been studied. In Appendix B we develop an approximate treatment of this effect based on Elmegreen's ideas in order to estimate the heating rate. The expression obtained there is again parameterized by an unknown efficiency factor that expresses the incomplete nature of theories of wind-disk mixing layers. At the likely efficiency of wind-disk heating, we find that it may be competitive with the viscous accretion heating discussed in the previous subsection. We also find that wind heating and accretion heating have other similarities. Both rates are proportional to the overall accretion rate and have the same dependence on the radial coordinate.

One issue that we cannot address without a more fundamental treatment of the mixing layer is how wind-disk heating depends on the vertical variation of the gas density. Our main conclusion is that it is a viable candidate for the heating of the upper layers of disks, but because of the similarities just noted, it may be hard to disentangle from accretion heating until a better theory becomes available. At this juncture, we adopt the view that equation (12) is a general surface heating formula

[2] The energy to make an He^+ ion in a cosmic gas is an order of magnitude larger than to make H^+ or H_2^+ because the He abundance is 0.1 that of hydrogen and because the electronic ionization cross section of He is somewhat smaller than that of atomic H.

[3] To anticipate the results presented below, a suitable choice for the surface regions may be $\alpha_h \sim 1$. Since they constitute a very small fraction of the surface density, accretion through these regions should not affect much the total accretion rate onto the star or the associated UV excess.

with a phenomenological coefficient α_h, whose origin may be viscous accretion, wind-disk interaction, or some other appropriate dissipative process.

2.5. *Line Cooling*

In the previous subsections we discussed several important heating and cooling processes for inner disk protoplanetary atmospheres, and now we consider line cooling. Since T_g ranges from $\sim$100 to $\sim$5000 K, the potential coolants range over almost the entire gamut of species familiar from the ISM. However, only a few of them will actually be effective in this problem. The mechanisms that produce more than 1% of the total heating and cooling rates are:

Heating:
- X-rays
- Accretion
- Wind-disk mixing layer.

Cooling:
- Dust-gas collisions
- Lyα
- Recombination lines
- O I forbidden lines
- O I fine-structure lines
- CO rotational lines
- CO rovibrational lines.

Appendix C describes how the line cooling rates are calculated.

3. CHEMISTRY

Disk surface chemistry is determined by the local gas density and temperature and by the intensity of the ionizing and dissociating radiation. The most important source of ionization for the inner disk is the X-rays emitted by the YSO (G97; IG99). X-ray–generated secondary electrons also dissociate molecules. Galactic cosmic rays are less important because they are largely excluded from the inner disk by the magnetized wind from the star-disk system (G97). Stellar and interstellar UV radiation are also more strongly attenuated in the inner disk than the X-rays owing to dust and self-shielding. However, both cosmic rays and UV radiation field can play important roles in the outer disk (Aikawa & Herbst 1999; Willacy & Langer 2000; Kamp et al. 2003; Bergin et al. 2003).

Because the chemistry is just one part of the broader thermal-chemical calculation, we do not have the luxury of working with a large chemical network, as is the practice in interstellar chemistry. Instead, we have developed a compact chemical model that incorporates the species and reactions that are important for gaining a preliminary understanding of the ionization and chemical structure of the atmosphere. We further restrict the analysis to gas-phase reactions, both neutral and ionic. Our chemical model is most appropriate where both the gas and dust are warm, so that the species do not stick to or react with the dust grains. In practice, this restricts us to $N_\perp < 10^{23}$–10^{24} cm^{-2}. At greater depths, we also cannot ignore X-ray scattering (IG99). The species in the model are:

H, H_2, H^+, H_2^+, H_3^+
He, He^+
O, OH, O_2, O_2H, H_2O, O^+, OH^+, H_2O^+, H_3O^+, O_2^+, O_2H^+
C, CO, C^+, HCO^+
A, A^+, e, where A stands for a generic neutral atom (Na).

Accompanying these 25 species are six conservation equations (for each nuclide and for charge) and about 115 reactions. Most of these reactions are ion-molecule reactions familiar from the chemistry of cool clouds (e.g., UMIST). In the following paragraphs, we emphasize the two most critical parts of the chemistry: the formation of H_2 and the synthesis by neutral reactions of simple molecules of thermodynamic or observational significance, especially CO. Ion-molecule reactions play a role because the X-rays irradiate the disk surface layers, but they serve mainly as mechanisms for molecular destruction.

In order to numerically solve the thermal-chemical problem defined in this and the previous sections, we divide the disk atmosphere into 150 layers. The steady thermal balance and chemical rate equations are solved iteratively by adopting a starting value for the temperature of a layer and solving the chemical equations by Newton's method. This solution is then used in the thermal balance equations to get a new value for the temperature. The process is repeated until the maximum relative difference between iterations is less than 10^{-8}. The values found for one layer are used as starting values for the next. Convergence of the temperature is reached after six iterations, whereas the solution of the chemical rate equations requires 15 iterations.

The wide variation in physical properties of the atmosphere demands special care in solving the chemical rate equations. Many of the chemical abundances vary rapidly and by many orders of magnitude, and it is necessary to work with more significant figures than the 16 normally given in double precision. We use a FORTRAN code that can solve the thermal-chemical equations with 30 significant figures. Typically it takes about 1 hr to solve an atmosphere using a Linux work station.

The chemical processes in the surface layers of the inner protoplanetary disk are affected by the large range in density and temperature encountered in disk atmospheres. In § 4 we will find that near 1 AU the gas density spans a range from $n_{\rm H} = 10^6$ to 10^{12} cm^{-3} while the temperature varies from $T_g \simeq 5000$ K at high altitudes to a minimum temperature $T_g \sim T_d \sim 150$ K between 2 and 3 scale heights. These ranges shift to somewhat higher or lower values within or beyond 1 AU. The large variation in temperature has several important effects on the chemistry. For example, the molecule that usually forms first on entering a region of increasing density is H_2. The standard way of forming H_2 in the ISM via grain synthesis (e.g., Hollenbach & Salpeter 1971) requires relatively cool conditions; otherwise, the H atoms do not stick on the dust surfaces long enough to form molecules.[4] In the absence of efficient grain synthesis, we invoke gas-phase processes, H^- formation,

$$e + {\rm H} \rightarrow {\rm H}^- + h\nu, \quad {\rm H}^- + {\rm H} \rightarrow {\rm H}_2 + e, \tag{15}$$

and three-body reactions,

$$3{\rm H} \rightarrow {\rm H}_2 + {\rm H}, \quad 2{\rm H} + {\rm H}_2 \rightarrow 2{\rm H}_2, \tag{16}$$

the latter accompanied by collisional dissociation,

$${\rm H} + {\rm H}_2 \rightarrow 3{\rm H}, \quad {\rm H}_2 + {\rm H}_2 \rightarrow {\rm H}_2 + 2{\rm H}. \tag{17}$$

Although both formation pathways depend on T_g, the most temperature-sensitive reactions are for collisional dissociation H_2, which are suppressed at low T_g. Complete conversion of atomic to molecular hydrogen at $\varpi = 1$ AU does not occur until $N_{\rm perp} \simeq 6 \times 10^{21}$ cm^{-2}, as a result of three-body formation. The H^- pathway is significantly diminished by photodissociation of H^- at high altitudes, but enough H_2 is synthesized to produce substantial OH and CO there.

[4] Cazaux and Tielens have recently argued that the grain synthesis may occur at dust temperatures as high as 200 K.

TABLE 1

Neutral Reactions

Reactants	Products	Rate Coefficient	At 500 K	At 5000 K
$O + H_2$	$OH + H$	$8.5 \times 10^{-20} T^{1.67} e^{-3163/T}$	4.9×10^{-18}	6.8×10^{-14}
$H + OH$	$O + H_2$	$8.1 \times 10^{-21} T^{2.80} e^{-1950/T}$	5.9×10^{-15}	1.2×10^{-10}
$OH + H_2$	$H_2O + H$	$1.7 \times 10^{-16} T^{1.6} e^{-1660/T}$	3.5×10^{-12}	1.0×10^{-10}
$H + H_2O$	$OH + H_2$	$7.5 \times 10^{-16} T^{1.6} e^{-9270/T}$	1.4×10^{-19}	9.7×10^{-11}
$O + OH$	$O_2 + H$	$2.0 \times 10^{-11} e^{112/T}$	2.5×10^{-11}	2.0×10^{-11}
$H + O_2$	$OH + O$	$3.3 \times 10^{-10} e^{-8456/T}$	1.5×10^{-11}	6.1×10^{-11}
$C + OH$	$CO + H$	1.6×10^{-11}	1.6×10^{-11}	1.6×10^{-11}
$H + CO$	$OH + C$	$1.6 \times 10^{-11} e^{-77,500/T}$	Negligible	3.0×10^{-18}
$C + O_2$	$CO + O$	3.3×10^{-11}	3.3×10^{-11}	3.3×10^{-11}
$O + CO$	$O_2 + C$	$3.3 \times 10^{-11} e^{-69,500/T}$	Negligible	3.0×10^{-17}
$OH + OH$	$O_2 + H_2$	$2.5 \times 10^{-15} T^{1.14} e^{-50/T}$	2.7×10^{-12}	4.1×10^{-11}
$O_2 + H_2$	$OH + OH$	$3.16 \times 10^{-21,900/T}$	Negligible	4.0×10^{-14}

Note.—Rate coefficient units are $cm^3\ s^{-1}$.

The formation of heavy molecules occurs through neutral radical and ion-molecule reactions, with the former being more important in warm layers at high altitudes and the latter in cool regions below. This kind of mixed chemistry is also characteristic of shocks and outflows from both YSOs and evolved stars. The neutral path to heavy molecule formation provides another illustration of the sensitivity of the chemistry to the temperature variation in the upper disk atmosphere. The slowest ("rate limiting") reaction is

$$O + H_2 \rightarrow H + OH. \tag{18}$$

Reasonably efficient for $T_g \geq 250$ K, this reaction leads to formation times longer than characteristic accretion times at lower temperatures. Once OH is formed, heavier molecules are rapidly synthesized by the reactions in Table 1, which updates those used by Glassgold et al. (1991) for YSO wind chemistry.

4. RESULTS

4.1. *Thermal Results*

Figure 1 plots the density in the D'Alessio et al. (1999) model versus height z at $\varpi = 1$ AU. We have added several values of the perpendicular column density $N_\perp$ to give an idea of the amount of material above a height z. In Figure 2, the dashed curve is the D'Alessio model temperature, which we identify as the dust temperature. In this and all of the following figures, we use the vertical or perpendicular column density instead of height z to convey the thermal (and chemical) structure of the atmosphere,

$$N_\perp(r,\ z) \equiv \int_z^\infty dz'\, n_{\rm H}(r,\ z'). \tag{19}$$

Because the temperature in the D'Alessio model varies with height (see the inversion or rise in temperature in Fig. 1 going from the midplane to the top of the atmosphere), the density profile in Figure 1 (for $r = 1$ AU) is a steep power law in z rather than a Gaussian. Figure 2 also plots our calculated gas temperatures (for the same value of r) for a range of α_h, the surface heating parameter defined in equation (12). The gas temperature has been calculated self-consistently with the chemical model presented in § 3. The rates for the heating and cooling processes are plotted in Figure 3 for the case $\alpha_h = 1$, and the abundances of the main species are shown in Figures 4 and 5, all for $r = 1$ AU.

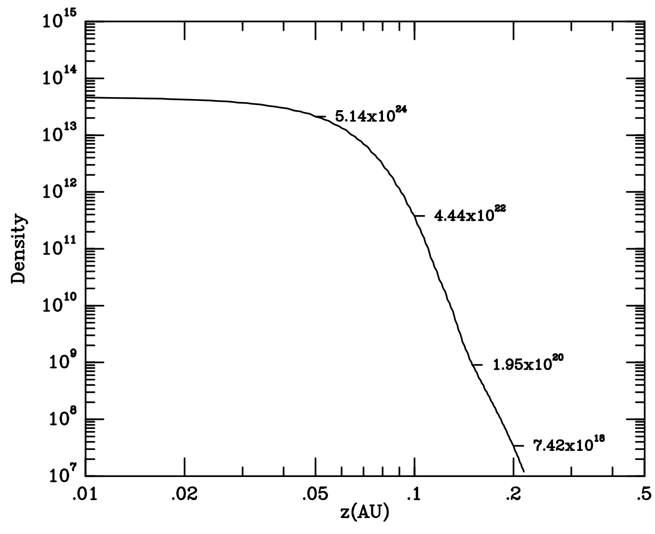

Fig. 1.—Volumetric gas density $n_{\rm H}$ plotted vs. height in AU at a radial distance of 1 AU, based on the disk model of D'Alessio et al. (1999). Several values of the vertical column density, measured from the top of the atmosphere in units of cm^{-2}, have been added to the curve. The analysis of this paper deals with the upper atmosphere where the density varies approximately as a power law.

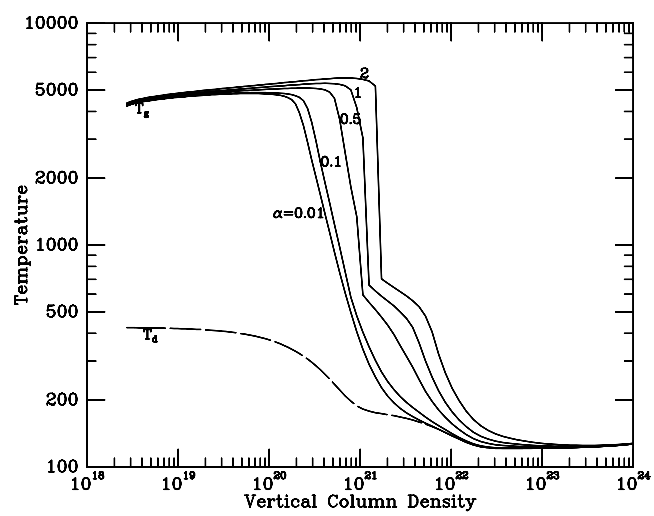

Fig. 2.—Gas and dust temperatures vs. perpendicular column density. The gas temperature has been calculated for a range of α_h (defined in eq. [12]) from 0.01 to 2. The radial distance is 1 AU. The dust temperature comes from D'Alessio et al. (1999).

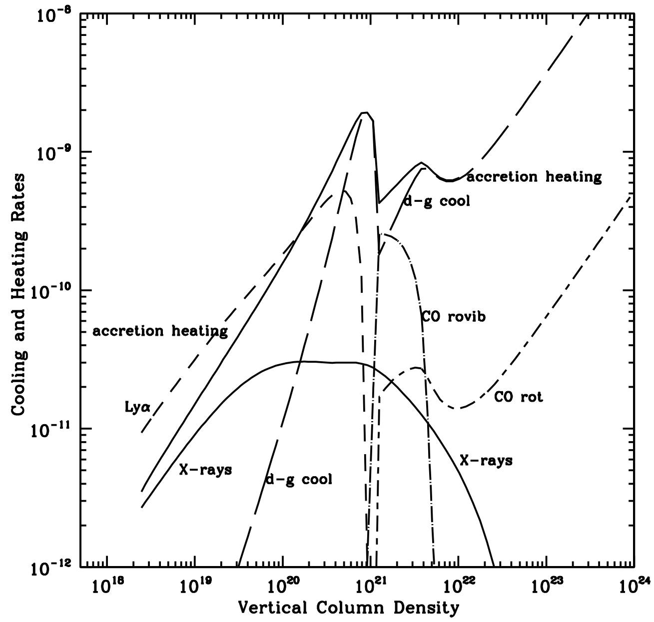

FIG. 3.—Heating and cooling rates vs. perpendicular column density at a radial distance of 1 AU for the case $\alpha_h = 1$. Heating rates are plotted by solid lines and cooling rates by dashed lines. The curve labeled "d-g cool" is the *net* dust-gas cooling, eq. (6).

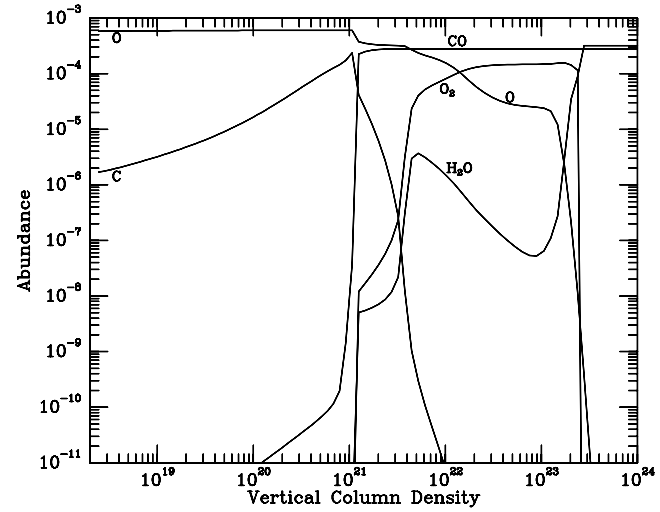

FIG. 5.—Abundances of the main oxygen species plotted vs. perpendicular column density at a radial distance of 1 AU for the case $\alpha_h = 1$.

As shown in Figure 2, high up in the atmosphere, $T_g \gg T_d$. Deeper down, at a depth (or vertical column) that increases with α_h, T_g drops rapidly and then gradually approaches T_d. Thus, the gas above the dust inversion layer consists of a hot layer on top of a warm layer. This double-layer structure occurs within the envelope of the density distribution of Figure 1, i.e., where the power law holds. Its existence can be understood by considering the variation of the heating and cooling rates and chemical abundances as a function of vertical column density (Figs. 3–5, all for the case $\alpha_h = 1$). The large temperatures at high altitudes are due to a combination of X-ray heating (lower solid curve in Fig. 3, dominant at small α_h) and accretion heating (upper solid curve in Fig. 3, dominant at large α_h) balanced by Lyα and O I forbidden line cooling. The rapid drop in T_g and its asymptotic approach to T_d are driven by the combined effects of the gas cooling by collisions with dust and CO line cooling. However, the rate of decrease and the thickness of the transition region between hot and warm layers are also strongly affected by the level of accretion-related heating, as is most evident from the shift of the curves in Figure 2 to large depths with increasing α_h.

The several cases displayed in Figure 2 show how the temperature profiles change as the role of accretion heating is increased relative to X-ray heating. For $\alpha_h = 0.01$, X-ray heating is dominant until $N_\perp \sim 10^{22}$ cm^{-2}, at which point the gas temperature approaches the dust temperature. The variation in X-ray heating with height is shown in Figure 3. X-ray heating first increases with $N_\perp$ as a result of the increase of hydrogen density with depth, but then it levels off and decreases as the X-rays are attenuated. At a larger value of $\alpha_h = 0.1$, the temperature profile and thermal balance are quite similar (Fig. 2), although accretion heating begins to compete with X-ray heating in the transition region. In both cases the transition region where $T_g \sim 500$–2000 K has a thickness, $\Delta N_\perp \sim 5 \times 10^{20}$ cm^{-2}. These small-α_h cases closely approximate the situation without any accretion heating and demonstrate that X-ray heating alone generates a significant zone of intermediate-temperature gas (Glassgold & Najita 2001).

Once $\alpha_h > 0.1$, we begin to approach the other extreme of negligible X-ray heating. For these cases, the intermediate-temperature transition regions in Figure 1 have a thickness $\Delta N_\perp > 10^{21}$ cm^{-2}. The temperature profiles also have an interesting "shoulder" between the sudden drop from large T_g at high altitudes to $T_d = 600$–700 K at $(1$–$2) \times 10^{21}$ cm^{-2}, followed by a slower decline down to T_d deep in the atmosphere. This behavior can be understood by referring to the thermal rates in Figure 3 and the chemical abundances in Figure 4. In Figure 3 for $\alpha_h = 1$, we see that the initial temperature drop at $\sim 10^{21}$ cm^{-2} occurs when the net dust-gas cooling overtakes both Lyα cooling and the dominant accretion heating. This behavior stems from the quadratic dependence of dust-gas cooling on the density compared to the linear dependence of the heating mechanisms. The decline in temperature also reflects an important chemical change, the formation of CO (see Fig. 4). CO rovibrational (and farther down CO rotational) cooling plays an important role in the transition region. Without it, dust-gas cooling, balanced by accretion

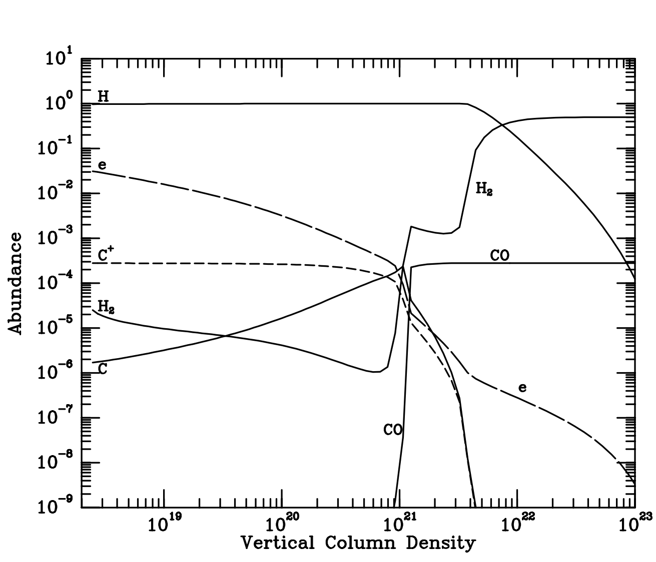

FIG. 4.—Abundances of H_2 and CO plus closely related species plotted vs. perpendicular column density at a radial distance of 1 AU for the case $\alpha_h = 1$.

heating, would produce a gradual transition. The presence of CO cooling produces the very sharp drops at $(1\text{–}2)\times10^{21}$ cm^{-2} for $\alpha_h \geq 0.5$; it also produces the shoulders in Figure 2 before T_g assumes its more gradual approach to T_d dictated by the dust-gas interaction. This result follows from our self-consistent calculation of thermal and chemical effects, whereby the formation of CO is accelerated by the drop in temperature, which in turn generates more cooling.

Some insight into the temperature profiles for finite α_h can also be gained from the following analytic solution for the case in which the only heating is from accretion and the only cooling is from collisions with dust:

$$T_g = T_d\left(\frac{1+\sqrt{1+J^2T_d}}{\sqrt{J^2T_d}}\right)^2, \tag{20}$$

where

$$J = \frac{n_\mathrm{H}}{2.08\times10^{15}\ \mathrm{cm}^{-3}}\frac{b}{\alpha_h} \tag{21}$$

and

$$b = \frac{m}{m_\mathrm{H}}\left(\frac{\rho_d}{\rho_g}\right)_{0.01}\left(\frac{0.05\ \mu\mathrm{m}}{a_g}\right)\left(\frac{\mathcal{A}_\mathrm{H}}{0.5}\right). \tag{22}$$

Equation (20) contains only one parameter, J^2T_d, and leads to a relatively gradual decline of T_g with depth, nothing like the sharp drop seen for $\alpha_h \geq 0.5$. The details of the calculated profiles shown in Figure 2 require additional coolants, especially CO rovibrational cooling. Equations (21) and (22) suggest that, to the extent that this simplified analytic model expresses the real situation, the choice of the accretion heating parameter α_h is affected by the dust model used for the dust-gas cooling through the factor b/α_h in equation (21). Thus, if the dust surface area is smaller than we have assumed, smaller values of α_h would be needed to give curves similar to those in Figure 2.

We carried out calculations at both smaller ($\varpi = 0.5$ AU) and larger ($\varpi = 2.0$ AU) radii and find qualitatively similar results. The temperature profiles have the same qualitative shape as those shown in Figure 2 for $\varpi = 1$ AU, indicating that the structure shown in Figure 2 is characteristic of a broader range of radii.

4.2. *Chemical Results*

Our thermal-chemical model produces a layered structure with a hot atomic region at the surface. At lower cooler depths, chemical transitions occur that convert the atomic into molecular gas. Figure 4 shows how the abundances of some important species vary with vertical column density for the case $\alpha_h = 1.0$. The first step is the synthesis of enough H_2 to form OH and CO. We have already noted how the rise in the CO abundance affects the transition between the hot and warm regions through the onset of rovibrational and rotational cooling. The CO abundance rises rapidly in the transition zone where T_g drops below 5000 K as a result of the shutdown of the inverse-synthesis reaction, H + CO → C + OH. Its formation at warm temperatures via neutral reactions requires that H_2 is also synthesized under these conditions since the precursor OH radical derives from H_2 (eq. [18]). H_2 is made first by the H^- reaction (eq. [15]) and then by three-body reactions (eq. [16]). Although hydrogen is at first mainly atomic, abundance levels $x(H_2) \sim 10^{-3}$ are more than sufficient to form OH and then CO. Essentially all of the available carbon is in CO when $N_\perp \simeq 1.25\times10^{21}$ cm^{-2} and $T_g = 650$ K.

The incorporation of all the available carbon into CO is the first *complete* chemical transition, and it occurs in a warm region that is mainly atomic. Most interesting from the observational perspective is the prediction of a significant column ($N_\perp \simeq 5\times10^{21}$ cm^{-2}) of warm CO ($T_g > 400$ K) in a region where atomic hydrogen dominates over molecular. Somewhat deeper down, essentially all of the available hydrogen is incorporated into H_2 in a moderately warm layer. Full association into H_2 does not occur until $N_\perp = 6\times10^{21}$ cm^{-2}, where the density is high enough ($n_\mathrm{H} = 5\times10^{10}$ cm^{-3}) for three-body reactions to be efficient and the temperature low enough ($T_g = 250$ K) for collisional dissociation to be unimportant. This second chemical transition is accompanied by the production of more OH and the synthesis of O_2 and H_2O, again with neutral reactions. The complete conversion of the residual oxygen in the form of O and O_2 into H_2O does not occur in the case shown in Figure 5 until $N_\perp \sim 4\times10^{23}$ cm^{-2} and $T_g \approx 125$ K. At these depths, however, our chemistry begins to break down because of the neglect of grain processes, as discussed earlier, and because some of the chemical timescales are approaching dynamical ones.

Figure 4 also shows how the electron fraction varies with $N_\perp$. The principal ions are H^+ for $N_\perp < 3\times10^{21}$ cm^{-2} and Na^+ for $N_\perp > 3\times10^{21}$. The abundances of C^+ and H^+ are about the same in the interval $N_\perp = 10^{21}\text{–}10^{22}$ cm^{-2}. The most abundant molecular ions are HCO^+, H_3O^+, and H_3^+. They peak in this same interval, where the hydrogen volume density is $\sim10^{10}$ cm^{-3}, with maximum abundances, respectively, of $\sim10^{-9}$, 8×10^{-10}, and 4×10^{-11}. Larger abundances would have been obtained if we had used a smaller Na abundance than our adopted value of $x_\mathrm{Na} = 10^{-6}$. Proton transfer and charge exchange with Na (and other neutral) atoms transfer ionization from hydrogenated ions and molecular ions to Na^+, which recombines slowly by radiative recombination.

Although Figures 4 and 5 present calculations only for $\alpha_h = 1$, the results are similar as long as α_h is not much larger than unity. For example, the location of the H → H_2 transition is $N_\perp = 7.5\times10^{21}$ cm^{-2} for the entire range $0.01 < \alpha_h < 2$. However, when $\alpha_h \gg 1$, the increased accretion heating becomes so strong that T_g in the upper atmosphere reaches values higher than 5000 K, e.g., 7500 K for $\alpha_h = 10$. This has the effect of increasing the relative importance of all of the inverse reactions in Table 1 and shifts the full association of atoms into molecules to larger depths.

5. DISCUSSION

In the previous sections we described a model for the thermal and chemical structure of gaseous disk atmospheres at AU radial distances. We found that X-rays, coupled with accretion-related heating processes, can produce warm surface layers in the gaseous atmosphere ($\sim$500–5000 K at $N_\perp = 10^{21}$ cm^{-2} for $\alpha_h \sim 0.1\text{–}1$). Although grains are likely to sediment out of the disk atmosphere on short timescales, we nevertheless find that molecules such as CO and H_2 are able to form in the atmosphere even in the absence of a grain population suitable for surface formation. The conversion of atomic to molecular hydrogen is driven initially by H^- at the disk surface and by three-body processes at higher column densities. Molecules such as CO form efficiently through neutral reactions even when the H_2 abundance is low. As a result, the transition from atomic carbon to CO occurs higher up in the atmosphere than the transition from atomic to molecular hydrogen. It is interesting to compare these specific features of our model with results from spectroscopic studies of inner disks.

A recent study of 4.7 μm CO fundamental line emission in classical T Tauri stars has found that fundamental emission is very common: CO fundamental lines are detected in $\gtrsim$80% of the classical T Tauri stars studied (Najita et al. 2003). The symmetric centrally peaked profiles of the CO fundamental lines, along with the profile widths ($\sim$70 km s^{-1}), suggest that the emission arises from a wide range of disk radii, from the inner disk edge at $\sim$0.04 AU out to 1–2 AU, i.e., in the terrestrial planet region of the disk. The relative strengths of the emission lines indicate that the emission originates from gas that is significantly warmer on average ($\sim$1000–1500 K) than the expected dust temperature at AU distances.

Our model appears to provide an explanation for the existence of warm CO in these disks. The processes that heat the gaseous disk atmosphere produce substantial column densities ($\gtrsim 10^{21}$ cm^{-2} at 1 AU) of warm ($\gtrsim$1000 K) gas in the upper atmosphere. The slowest reaction involved in the formation of CO (eq. [18]) is reasonably efficient, and atomic carbon is converted to CO at a column density of $\sim 10^{21}$ cm^{-2}, i.e., at a column density where the gas temperature is $\sim$1000 K. In comparison, the dust temperature at a column density of $\sim 10^{21}$ cm^{-2} at 1 AU is much lower, $\sim$200 K (Fig. 1).

Another aspect of the CO fundamental observations that is perhaps surprising is that the vibrational levels of CO are so well excited at temperatures $\lesssim$1500 K. At these low temperatures, chemical equilibrium would predict that most of the hydrogen would be in molecular form at the high characteristic density of the disk (e.g., Najita et al. 1996). This situation is not advantageous for exciting the CO vibrational transitions since the cross section for exciting CO via collisions with H_2 is much smaller than the cross section for exciting CO with atomic hydrogen. In contrast, in our models we find that the layered vertical structure of the disk permits an interesting situation: the C/CO transition is made at low H_2 abundance so that CO coexists with atomic hydrogen over a large column density. The intermixing of CO with atomic hydrogen in the warm upper atmosphere is advantageous for the excitation of CO and may partly explain the frequent detection of CO fundamental emission.

The observed strength of the CO fundamental emission from classical T Tauri stars is also found to be correlated with the accretion rate onto the star, suggesting that accretion plays an important role in heating the emitting gas (Najita et al. 2003). This is consistent with the theoretical results obtained here. We find that accretion-related processes such as viscous dissipation and wind interactions can significantly enhance the heating of the disk atmosphere above a minimum level established by X-ray irradiation, producing large column densities of warm molecular gas ($\gtrsim 10^{21}$ cm^{-2}) that are comparable to the observed CO column densities.

Additional observational support for the role of accretion-related processes in heating the disk atmosphere comes from the intrinsic line profiles of the CO overtone lines, which probe the region $\sim$0.04–0.3 AU in T Tauri disks. Spectral synthesis modeling of the CO overtone lines shows that the lines experience suprathermal intrinsic line broadening (Carr et al. 2004; Najita et al. 1996). The overtone lines are particularly sensitive to the width of the intrinsic line profile because the close overlap of lines near the band head makes it possible to distinguish between intrinsic line broadening and broadening due to macroscopic motion such as rotation. Possible explanations for the enhanced line width include turbulence associated with in situ angular momentum transport (e.g., via the magnetorotational instability [Balbus & Hawley 1991] or the global baroclinic instability [Klahr & Bodenheimer 2003]) or turbulence induced at the disk surface by a wind blowing over the disk. The turbulence in these scenarios is driven by accretion.

Finally, the observation that CO fundamental emission is commonly detected from both single and binary classical T Tauri stars (Najita et al. 2003) may provide a clue to the dominant heating processes in disk atmospheres. Whereas line emission from disks around single stars is believed to arise from a temperature inversion region in the disk atmosphere, stellar companions if present may carve out "gaps" in the disk in the vicinity of the binary orbit, creating low column density regions that may also contribute to line emission. The CO fundamental observations suggest that both disk atmospheres and gaps produce strong emission, with a remarkable similarity between the CO line profiles measured for binaries and single stars (with the notable exception of GW Ori), which indicates that the emissions from atmospheres and gaps are similar.

What does this suggest about the dominant heating processes in disk atmospheres? We have identified X-ray irradiation, viscous accretion, and wind-disk interaction as potential heating processes. All of these processes may play a role in heating the atmospheres of disks around single stars. However, it seems unlikely that the same form of viscous accretion is responsible for heating any residual, low column density gas within disk gaps. While gas may cross gaps in accretion streams (Artymowicz & Lubow 1996), the process by which the accretion energy is dissipated is probably quite different from disk accretion around single stars. Therefore, the close similarity between the line profiles of single and binary stars may be suggesting that viscous accretion is not the dominant heating process in disk atmospheres. In comparison, both X-ray irradiation and wind-disk interaction would heat disk atmospheres and residual gas in gaps in similar ways; perhaps they are the dominant heating processes in gaps.

Additional evidence for warm gaseous atmospheres in inner disks comes from the observation of UV fluorescence from H_2 in the 1250–1650 Å band from the $\sim$10 Myr old T Tauri star TW Hya (Herczeg et al. 2002). An analysis of the spectrum shows that photons in the wings of the stellar Lyα line excite warm ($\gtrsim$2000 K) H_2 gas, producing the observed downward cascade. The characteristic H_2 column density of the emission is modest, $\sim 10^{18}$ cm^{-2}. Since the H_2 emission is spatially unresolved, it must originate from within 1.4 AU of the star, approximately the same region probed by the CO fundamental lines.

While similarly warm ($\sim$1000 K) molecular gas is expected in our model, the UV excitation of H_2 may, at first, appear to be surprising given the column depth at which we expect H_2 to form. In our model, an H_2 column density of 10^{18} cm^{-2} is reached at a total hydrogen column density of $\sim 10^{21}$ cm^{-2} (where the fractional abundance of H_2 is 10^{-3}). In order to excite the H_2 emission, the Lyα photons must penetrate this relatively large column. Since Lyα radiation is typically scattered and absorbed by dust over much smaller characteristic column densities, the detection of Lyα-excited H_2 emission suggests that the dust absorption column density to the H_2 formation depth is low. This would be consistent with the expectation of significant grain growth and settling in a disk that is 10 Myr old. Perhaps not surprisingly, the spectral energy distribution for this source indicates just such a deficit of grain opacity in the region inside 4 AU (Calvet et al. 2002). Our proposed explanation of the Lyα pumped H_2 emission may not apply to similar observations of classical T Tauri stars (Valenti et al. 2000; Ardila et al. 2002). Various properties of the observed emission from these sources suggest that the emission in these objects arises in winds rather than disks.

Our finding that a large total column of gas is required to convert atomic to molecular hydrogen illustrates how models of gaseous disk atmospheres are necessary to extract total gas masses from spectral line observations. Again TW Hya provides a good example. Here the small H_2 abundance in the warm transition region of our model implies that a significant amount of gas remains in the terrestrial planet forming region of this system, despite the low IR excess. The presence of a significant gas reservoir is consistent with the detection of ongoing accretion onto the star, e.g., as indicated by broad hydrogen line profiles and UV excess emission (Muzerolle et al. 2000). A gas-rich, inner disk with a low continuum opacity is also the situation expected in the initial planet-building stage of the core accretion model. Of course, it would be important to determine from detailed modeling just how much gas is left in this region. For example, if the TW Hya disk is actively building terrestrial planets, the residual gas content may affect the ultimate mass and eccentricity of the planets and their consequent habitability (e.g., Kominami & Ida 2002). To address this issue, models of the kind presented here can be used to convert measured line diagnostics into total gas column densities.

In making such a conversion (e.g., in the absence of the kind of models presented here), one might be tempted to assume that the formation depth of H_2 is determined by the column density required to shield H_2 from the dissociating far UV radiation field. For diffuse interstellar clouds with densities of $\sim$100 cm^{-3}, the shielding column is $\sim 10^{20}$ cm^{-2} (Spitzer & Jenkins 1975). However, this column is a sensitive, decreasing function of density because the photodissociation of H_2 proceeds via line absorption, and it is a nonlinear function of density and to a lesser extent of temperature (Federman et al. 1979). At the much higher densities of the disk atmospheres considered here, the corresponding UV shielding column might be expected to be small. In contrast, in our calculations, we find that hydrogen is not fully associated into H_2 until large column densities are reached. Even at $N_{\rm H} \simeq 1\times 10^{21}$ cm^{-2}, the fractional abundance of H_2 is only 10^{-3}, primarily because of the effects of X-ray irradiation by the central star rather than by dissociation via UV line absorption.

Although the models we have described here apply specifically to large column density, optically thick disks, similar models are likely to apply to disks with low continuum opacities (e.g., those in which grain growth is advanced), as well as to low column density regions in disks (e.g., to disk gaps or regions in which disk dissipation is advanced). Again, the region of the TW Hya disk responsible for the H_2 UV fluorescence provides a good example. TW Hya has a modest accretion rate (4×10^{-10} $M_\odot$ yr^{-1}; Muzerolle et al. 2000), so accretion-related heating of the disk may be relatively weak (see, however, Alencar & Batalha 2002, who determine a larger accretion rate of 10^{-9} to 10^{-8} $M_\odot$ yr^{-1} for this source). The temperature of the H_2-emitting gas is 2000–3500 K (Herczeg et al. 2002), at the upper end of the temperature range calculated from our model at 1 AU for an accretion rate of 10^{-8} $M_\odot$ yr^{-1}.

The higher H_2 emission temperature may result from the low grain abundance in the inner disk of TW Hya (Calvet et al. 2002), which would have the effect of reducing the dust-gas cooling, or it might stem from the lower disk density that would exist under hydrostatic equilibrium conditions, which would not only reduce gas-grain cooling but enhance the role of X-ray heating. Another possibility is that the emission arises predominantly from inside 1 AU, where the disk is warmer than at 1 AU. Yet another possibility is that an embedded protoplanetary companion, whose presence in the apparent gap is speculated upon by Calvet et al. (2002), causes significant additional heating of its surroundings. Thus, the TW Hya system poses interesting future challenges for our model and suggests the need for a more self-consistent density structure and potentially new heating and ionization sources.

Further work is also needed to understand the origin of water emission from inner T Tauri disks, e.g., the water emission lines in the *K* band that probe the region of the disk within $\sim$0.5 AU (e.g., Najita et al. 2000). A joint analysis of the CO and water emission spectrum of SVS 13 in this spectral region (Carr et al. 2004) indicates that the water-to-CO abundance ratio is much lower than would be expected in chemical equilibrium. Such large deviations may originate in the layered picture of the disk atmosphere described here, where molecular abundances are definitely nonequilibrium and vary strongly with depth. In the results presented here for the chemical structure of the disk at larger ($\sim$AU) distances, residual atomic oxygen forms molecules such as O_2 and H_2O beyond a column density of $\sim 10^{22}$ cm^{-2}, a much larger column density than the $\sim 10^{21}$ cm^{-2} column density at which CO forms. Since water forms much farther down in the atmosphere than does CO, a much smaller column density of water is likely to be present in the temperature inversion region of the disk. A similarly layered structure is likely to be present at smaller disk radii. Thus, it will be interesting to expand the present chemical model in order to study the chemistry at smaller disk radii and to make more detailed comparisons with relative molecular abundance measurements of disk atmospheres.

6. CONCLUSIONS

We have carried out a detailed, but still approximate, study of the thermal structure of gaseous disk atmospheres, including the effects of accretion-related heating processes and grain growth. We find that the regions where the gas and dust temperatures differ include the part of the disk atmosphere that is accessible to observational study. Thermal models that treat the gas and dust as completely thermally coupled are therefore incomplete with regard to the study of gas-phase diagnostics of disk atmospheres. Our work represents a first step in the development of models of the inner disk that treat the dust and gas as separate coupled systems.

Our current model suffers from several limitations. We may have overestimated the disk dust temperature since the dust temperature structure assumed here, the T Tauri disk model of D'Alessio et al. (1999), is based on (small) ISM-like grains rather than on the larger grains that are likely to exist in T Tauri disks. The magnitude of the overestimate is probably small, however, since models that incorporate larger grains predict temperature structures similar to the one assumed here (e.g., D'Alessio et al. 2001). Larger grains may be expected to lead to a reduction in dust-gas cooling, but this may be countered by the lower temperature of the grains and the possibility that the transition from high to low temperatures occurs at higher densities in disks with less flaring. It would be of considerable interest to extend the present calculations to grain size distributions with larger maximum sizes. Nonetheless, we expect that the model results obtained here should be representative of the general character of the gaseous atmosphere, e.g., the conclusion that the gas will be hotter than the dust in the inner disk is likely to be robust.

Another limitation of our present procedure is that hydrostatic equilibrium is not enforced. Since we start with the density and dust temperature distribution of the atmosphere calculated by D'Alessio et al. (1999), the gaseous atmosphere would be in hydrostatic equilibrium only if the gas and dust temperatures are equal. Instead, we find that the gas is warmer than the dust in the region of the inversion, so the atmosphere is denser in our models than it would be in equilibrium. More complete models should, therefore, treat the atmosphere as composed of two separate but interacting fluids, the gas and the dust, with the gas in hydrostatic equilibrium and the dust suspended to the extent allowed by grain growth and settling. Since such atmospheres would be more rarefied than assumed in the present calculation, the thermal decoupling of the gas and dust would likely be enhanced and gas cooling would be reduced, resulting in warmer gaseous disk atmospheres. On the other hand, models that take better account of grain settling and growth may also cause the dust irradiation surface (and the dust temperature inversion) to occur deeper in the atmosphere if the upper layers are depleted in dust (P. D'Alesssio 2004, private communication). This would then affect the gas temperature and be important for understanding gaseous tracers that form at large vertical column densities, such as water.

A possibly important inconsistency in our models is that we have assumed that the disk atmosphere is quiescent and vertically stratified in calculating its thermal and chemical properties, but we have also invoked accretion-related heating processes that are likely to be accompanied by significant turbulence and the potential for mixing of the layers. Models of gaseous atmospheres that resolve this inconsistency may be needed to make detailed comparisons with observations of disks undergoing accretion. These models are expected to be a significant theoretical challenge (see, e.g., Ilgner et al. 2004).

In analyzing the difference between the gas and the dust temperatures, we considered several unconventional heating mechanisms. First, we verified that X-rays do produce a large temperature inversion in the gaseous disk atmosphere, much larger than the temperature inversion experienced by the dust over the same column density. The vertical extent of the temperature inversion is larger if the two additional heating mechanisms we considered are operative. Both of these heating mechanisms are related to turbulent dissipation, one directly related to the viscous accretion process associated with angular momentum transport in the disk and the other with the interaction of the stellar outflow and the disk. When parameterized in terms of the standard rate of viscous dissipation (eq. [12]) using a phenomenological parameter α_h, we found that α_h must be large ($\sim$1) in order to explain the observation of abundant warm CO in the terrestrial planet region of classical T Tauri disks. Given that the current models are likely to underestimate the temperature of the gaseous atmosphere (see previous paragraph), improved models are likely to produce similar thermal-chemical structures with lower values of α_h.

What is the meaning of the value of α_h inferred in this way? As described in § 2, it may refer to heating produced by accretion in the disk atmosphere itself or by the shear flow of a wind blowing over the disk surface. It may also derive from heating produced by accretion flows below the disk atmosphere, which generate waves that propagate to the disk surface and dissipate there (Miller & Stone 2000). Yet another possibility is heating that derives from the presence of embedded companions, which can also generate waves that propagate into and dissipate in the disk atmosphere (D'Angelo et al. 2003; Lubow & Ogilvie 1998; Ogilvie & Lubow 1999). An important challenge to theory is to obtain detailed prescriptions for the heating produced by all of these mechanisms that could be used to create more accurate models of disk atmospheres.

It will be interesting, in future calculations that remove some of the above limitations, to explore the structure of disk atmospheres over a range of disk radii, as well as to study the formation of more complex molecules such as water. Water is expected to be a powerful probe of dense, warm gaseous disks at disk radii larger than those probed by the CO fundamental lines. Also important is the related issue of identifying useful spectral line diagnostics of regions of low continuum optical depth, i.e., disk gaps, dissipating disks, or regions in which grain growth is advanced, as discussed in § 5 in connection with the TW Hya system. Models of this type have recently been constructed, focusing primarily on the giant planet region of the disk (Gorti & Hollenbach 2004).

Similar models that focus on smaller disk radii are also of interest to help interpret existing observations. For example, CO fundamental observations of disks with low infrared excess have been used to study the gas dissipation timescale in the terrestrial planet region of disks (e.g., Najita 2004). Such observations address the question of whether gas persists after infrared excesses have disappeared and whether low infrared excesses are the result of disk dissipation or grain growth. Measurements of the gas dissipation timescale in the terrestrial planet region have the potential to address some important aspects of terrestrial planet formation. For example, residual gas in the terrestrial planet region of the disk may play an important role in determining the ultimate mass and eccentricity of a terrestrial planet (e.g., Kominami & Ida 2002) and its consequent habitability. Since systems with low infrared excess are typically also systems in which the accretion rate is low, these systems may be easier to model in that the current uncertainty in how to include the effects of accretion (i.e., what is the appropriate value of α_h?) will be less critical. It will, however, be important to include some of the model refinements discussed above (e.g., hydrostatic equilibrium) in order to convert reliably measured CO column densities (or upper limits) into total gas column densities.

The observational diagnostics that we have discussed in connection with our models appear to primarily probe large disk column densities $\gtrsim 10^{21}$ cm^{-2}. However, our models also predict a warm, $\sim$5000 K, atomic surface region ($\lesssim 10^{21}$ cm^{-2}) that is produced by X-ray heating. Identifying robust diagnostics of this region may prove useful for the study of dissipating (low column density) disks. Indeed, Gorti & Hollenbach (2004) predict that fine-structure lines are some of the strongest diagnostic features of dissipating disks. It would be useful to identify similar diagnostics that probe small disk radii in protoplanetary disks. In summary, improved models of gaseous disk atmospheres should be useful in understanding the structure and dynamics of the inner parts of disks that play a key role in star and planet formation.

The authors would like to thank Eugene Chiang, Bruce Elmegreen, and David Hollenbach for helpful conversations. They are indebted to Paola D'Alessio for providing the results of her calculations of disk atmospheres on which this work is based. This research has received support from NSF grant AST 00-97978 and NASA grant NAG5-12167.

APPENDIX A

DUST-GAS COOLING

In order to analyze the effects of grain size on dust-gas cooling, we average equation (2) over an MRN-type dust size distribution,

$$n_d(a) = C_p a^{-p}, \qquad a_1 < a < a_2, \tag{A1}$$

and zero outside the indicated range. The normalization factor is

$$C_p = \frac{\rho_d}{(4\pi/3)\tilde{\rho}} \frac{4-p}{a_2^{4-p} - a_1^{4-p}}, \tag{A2}$$

where ρ_d is the volumetric mass density of dust in the disk and $\tilde{\rho}$ is the internal density of a dust grain, assumed to be independent of size. The zeroth moment of equation (A1) is the total volumetric number density of dust grains,

$$n_d = \frac{4-p}{1-p} \frac{\rho_d}{(4\pi/3)\tilde{\rho}} a_2^{-3} \frac{(a_2/a_1)^{p-1} - 1}{1 - (a_1/a_2)^{4-p}}. \tag{A3}$$

In equation (2), the first term, proportional to T_g, involves the dust surface area per unit volume, which, on calculating the second moment for the MRN choice, $p = 3.5$, is

$$n_d \langle a^2 \rangle = \frac{\rho_d}{(4\pi/3)\tilde{\rho} a_g} \, a_g = (a_1 a_2)^{1/2}, \tag{A4}$$

where the angle brackets indicate a straight average with the MRN distribution, equation (A1). The mean surface area per unit volume is inversely proportional to the geometric mean of the minimum and maximum grain radii. The second term of equation (2) involves the mean temperature of a grain $T_d(a)$, which we calculate by balancing absorption and emission, ignoring the temperature fluctuations important for small grains. We assume that the absorption occurs at high frequency, where the absorption coefficient $Q_\nu \simeq 1$, and that the emission occurs at low frequencies, where $Q_\nu \propto \nu^\beta$ with $\beta \simeq 1$–2. This familiar approximation, used, for example, by Chiang & Goldreich (1997), holds at high disk altitudes not too close to the central star. Close in, where the grains can become quite warm, departures from these extreme assumptions can become important, especially in the context of grain heating by the diffuse infrared radiation field, as well as direct stellar optical radiation (Wolf 2003). In any case, our simplified treatment leads to a mean grain temperature,

$$T_d(a) \propto a^{-b}, \qquad b = \frac{\beta}{4+\beta}, \tag{A5}$$

which has an inverse size dependence with a small power index $b = \frac{1}{5} - \frac{1}{3}$ (if the index β of the absorption coefficient lies between 1 and 2). Thus, the second term in equation (2) involves the $(2-b)$-moment of the grain size distribution and emphasizes slightly smaller (and warmer) grains than the first term. The final result for the dust-gas heating rate with an MRN distribution with $p = 3.5$ and unspecified minimum and maximum grain sizes is

$$\Lambda_{dg} = \frac{\rho_d}{(4\pi/3)\tilde{\rho} a_g^3} n_{\mathrm{H}} \bar{v}(\mathrm{H}) 2\mathcal{A}_{\mathrm{H}} k \left(T_g - \bar{T}_d\right) \pi a_g^2, \tag{A6}$$

where

$$\bar{T}_d = B \langle T_d(a) \rangle, \qquad B = \frac{1 + 0.4b}{1 + 2b} \frac{1 - (a_1/a_2)^{0.5+b}}{1 - (a_1/a_2)^{0.5}}, \tag{A7}$$

and B is a number somewhat smaller than unity for grain distributions with $a_2/a_1 \gg 1$ and slightly greater than unity for a_2 comparable with a_1. In equation (A6), the quantity $\mathcal{A}_{\mathrm{H}}$ is the accomodation coefficient defined in equation (3), with a value $\sim$0.5.

APPENDIX B

WIND-DISK HEATING

We adopt the standard view that accretion through the disk of a YSO is accompanied by a bipolar wind that originates close to the star, perhaps from the inner edge of the disk as in an *X*-wind. In addition to a jet close to the rotational axis of the disk, the wind has a wide-angle component that interacts with a flaring disk. When it blows over the disk, it produces a turbulent mixing layer (called an "aeolosphere" by Carr et al. 1993). Our objective is to make an order-of-magnitude estimate to ascertain whether it is competitive with other mechanisms for heating the upper layer of a disk atmosphere.

We assume that the wind is radial with constant terminal velocity v_W and a possible angular dependence away from the jet region represented by a factor $F(\theta)$ in the wind hydrogen density,

$$\rho_W = \rho_0 F(\theta), \qquad \rho_0 = \frac{\dot{M}_W}{4\pi r^2 v_W}, \tag{B1}$$

where r, θ are spherical coordinates and F is normalized so that $\int_{-\pi}^{\pi} d\theta \, \sin\theta F(\theta) = 2$. The density of the equivalent spherical wind ρ_0 can be expressed numerically in terms of the number of hydrogen nuclei ($\rho_0 = 1.425 m_{\rm H} n_0$ using solar abundances),

$$n_0 = \left(9.4\times10^6 \ {\rm cm^{-3}}\right)\left(\frac{\dot{M}_{-8}}{v_{100}}\right)\left(\frac{\rm AU}{r}\right)^2, \tag{B2}$$

where $\dot{M}_{-8}$ is $\dot{M}_W$ in units of $10^{-8}\ M_\odot\ {\rm yr^{-1}}$ and v_{100} is v_W in units of 100 km s^{-1}.

Following Elmegreen (1978), we locate the upper and lower boundaries of the turbulent mixing layer by matching the normal and maximum wind pressure with the disk pressure. Thus, the upper boundary $z_2(\varpi)$ is defined by the "normal pressure balance,"

$$p_W + \rho_W v_W^2 \sin^2\alpha = p_D, \tag{B3}$$

and the lower boundary $z_1(\varpi)$ is defined by the "maximum pressure balance,"

$$p_W + \rho_W v_W^2 = p_D. \tag{B4}$$

The angle α is the "attack" angle of the radial wind on the upper surface $z_2(\varpi)$, and p_D is the disk atmosphere pressure field. The location of the lower surface is less secure than the upper since it depends on a real understanding of the development of the turbulent mixing layer, which we lack, but Elmegreen's choice should suffice for rough estimates. When we rewrite the left side of equation (B3) as $\rho_W(c^2 + v_W^2 \sin^2\alpha)$, we see that the ram pressure dominates for a sufficiently cool wind. This is likely to be the case for a wide-angle wind owing to adiabatic expansion cooling before it gets to skim the disk.

Given the run in disk pressure $p_D(\varpi, z)$, e.g., the table of numerical values provided by P. D'Alessio (2000, private communication), and the wind density (eq. [B1]), equation (B4) can be solved by interpolation on the pressure table. On the other hand, equation (B3) is essentially a differential equation for the surface $z_2(\varpi)$ (Elmegreen 1978). We can obtain this equation with the help of the angle θ tangent to the surface at (ϖ, z_2) and the angle $\beta = \arctan(z/\varpi)$. Since $\theta = \alpha + \beta$, $z_2(\varpi)$ satisfies the equation

$$\frac{dz_2}{d\varpi} = \frac{z_2}{\varpi} + \arcsin\left(\frac{p_D}{\dot{M}_W v_W^2}\right)^{1/2}, \tag{B5}$$

in the small α and β limit. Using equation (B4), this reduces to

$$\frac{dz_2}{d\varpi} = \frac{z_2}{\varpi} + \left\{\frac{p_D[z_2(\varpi)]}{p_D[z_1(\varpi)]}\right\}^{1/2}. \tag{B6}$$

The pressure ratio in the second term can be approximated for the D'Alessio et al. model by $(z_1/z_2)^m$, with $m \simeq 11$ near $\varpi = 1$ AU. An approximate analytic solution can then be found to this nonlinear equation that has $\alpha \to 0$ as $\varpi \to 0$. For a spherical wind with $\dot{M}_W = 10^{-8}\ M_\odot\ {\rm yr^{-1}}$ and $v_W = 200$ km s^{-1}, we find that around $\varpi = 1$ AU,

$$z_1 \simeq (0.112\ {\rm AU})\left(\frac{\rm AU}{\varpi}\right)^{1.16}, \qquad z_2 \simeq (0.213\ {\rm AU})\left(\frac{\rm AU}{\varpi}\right)^{1.135}, \tag{B7}$$

and

$$\alpha \simeq 0.029\left(\frac{\rm AU}{\varpi}\right)^{0.135}. \tag{B8}$$

In this case, the surface occurs at relatively high altitudes ($\sim 5H$ in terms of the midplane scale height H), the attack angle is small (~ 0.03 rad), and the thickness of the turbulent mixing layer is relatively large (~ 0.1 AU). For a more powerful wind, the surfaces are pushed down toward the midplane, the attack angle will be larger, and $z_2 - z_1$ will be smaller. Of course, all of these numbers are problematic in the absence of a real theory for the layer.

The basis for our estimate of wind-disk heating is a calculation of the wind mechanical energy that enters the disk. First consider a radial position ϖ where the wind-layer interface is at height $z_2(\varpi)$ above the midplane. At this point, the wind enters the layer at the angle α, the angle between $\hat{r}$ and the tangent to the surface $\hat{t}$ at fixed azimuthal angle ϕ. If ds is a line element of the surface along $\hat{t}$, then the solid angle subtended by ds at the origin, after integrating ϕ over 2π, is

$$d\Omega = \frac{2\pi\varpi\, ds \sin\alpha}{r^2}. \tag{B9}$$

If the tangent to the upper surface is β, then we can replace ds by $d\varpi$ using

$$\frac{ds}{d\varpi} = \sec\beta, \tag{B10}$$

so that

$$d\Omega = 2\pi \frac{\varpi}{r^2} \frac{\sin\alpha}{\cos\beta}\, d\varpi. \tag{B11}$$

In the inner disk we expect α and β to be small so that $\sin\alpha/\cos\beta \sim \alpha$. The mechanical luminosity incident on the layer within $d\Omega$ is

$$dL_{\rm mech} = \frac{1}{2}\rho_0 v_W^3 F(\theta) r^2\, d\Omega = \frac{1}{4\pi}\, d\Omega\, F(\theta) L_{\rm mech}, \tag{B12}$$

where we have used equation (B1) and introduced the total mechanical luminosity

$$L_{\rm mech} = \dot{M}_W \frac{v_W^2}{2}. \tag{B13}$$

We can obtain an approximate formula for the volumetric heating rate in the turbulent mixing later by assuming that (1) a certain fraction $\epsilon_{\rm mech}$ of the mechanical luminosity incident within a solid angle $\delta\Omega$ heats the layer and (2) this fraction is dissipated over a volume (after integrating over the azimuthal angle) defined by $\delta\varpi$ and δz. The interval $\delta\varpi$ is defined via equation (B10) in terms of the surface element ds, and the interval δz is taken to be $z_2(\varpi) - z_1(\varpi)$:

$$\delta V = 2\pi\varpi\, \delta\varpi\, \delta z = 2\pi\varpi \tan\beta\, \delta\varpi^2. \tag{B14}$$

We find from equations (B3) and (B4) that δz is of the order of 2 scale heights. The heating rate is

$$\Gamma_{\rm mech} = \epsilon_{\rm mech} \frac{\delta L_{\rm mech}}{\delta V}, \tag{B15}$$

which becomes, on substituting equations (B12), (B11), and (B1) and using $dz/d\varpi = \tan\beta$,

$$\Gamma_{\rm mech} = [\epsilon_{\rm mech} F(\theta) \sin\alpha\, \cos\beta] \frac{1}{2}\rho_0 \frac{v_W^3}{\delta z}. \tag{B16}$$

This formula has the expected form (and dimensions) for the dissipation rate of a wind, multiplied by factors that express the wind's angular dependence and angle of incidence and by an unknown efficiency factor.

For purposes of discussion, we introduce an overall efficiency factor,

$$\alpha_{\rm mech} = \epsilon_{\rm mech} F(\theta) \sin\alpha\, \cos\beta, \tag{B17}$$

which depends on where the wind enters the layer. Then the mechanical heating rate can be expressed as

$$\Gamma_{\rm mech} = \alpha_{\rm mech} \frac{1}{2}\rho_0 \frac{v_W^3}{\delta z} = \alpha_{\rm mech} \frac{\dot{M}_W v_W^2}{4\pi r^2}. \tag{B18}$$

Of the three factors that enter equation (B17) for $\alpha_{\rm mech}$, we know only that $\sin\alpha \ll 1$ ($\sim$0.03 according to earlier estimates) and that $\cos\beta \sim 1$. There is no direct observational evidence on the angular dependence of the wide-angle part of a YSO wind, although it probably carries away about half of the ejected mass. MHD wind theories (e.g., Najita & Shu 1994; Shu et al. 1995) suggest that the wind density does not vary much with angle at the small latitudes relevant for skimming the disk, so we guess that $F \sim 0.5$. Once the wind energy enters the mixing layer, we expect that a substantial fraction is dissipated, so that $\epsilon_{\rm mech}$ might lie in the range 0.01–0.1. Thus, we estimate that overall $\alpha_{\rm mech} \sim 10^{-4}$ to 10^{-3}, although obviously with much uncertainty.

For numerical purposes, equation (B18) can be written as

$$\Gamma_{\rm mech} = \left(7.49\times10^{-10}\ {\rm ergs\ cm^{-3}\ s^{-1}}\right)\alpha_{\rm mech} \frac{\dot{M}_{-8} v_{100}^2}{(r/{\rm AU})^2 (\delta z/{\rm AU})}. \tag{B19}$$

Substituting $\alpha_{\rm mech} = 10^{-3}$, $r = 0.1$ AU, $\delta z = 0.1$ AU, and $v_{100} = 2$ yields $\Gamma_{\rm mech} \sim 10^{-11}$ ergs cm^{-3} s^{-1} at 1 AU, which is competitive with the accretion heating of the last subsection. We can confirm this by rewriting the first form of equation (B18) with equation (B3) for normal pressure balance,

$$\Gamma_{\rm mech} = \frac{\epsilon_{\rm mech}}{\sin\alpha\, \cos\beta} \frac{p_D v_W}{\delta z}, \tag{B20}$$

and then using $p_D = \rho c^2$ and equation (12):

$$\Gamma_{\rm mech} = \frac{\epsilon_{\rm mech}}{\sin\alpha\,\cos\beta}\frac{H}{\delta z}(\rho c)_2\Omega, \tag{B21}$$

where the subscript 2 signifies evaluation at the upper boundary of the layer. We can compare this with the result of the previous subsection,

$$\Gamma_{\rm acc} = \frac{9}{4}\alpha_{\rm vis}\rho c^2\Omega,$$

to get

$$\frac{\Gamma_{\rm mech}}{\Gamma_{\rm acc}} = \frac{4}{9}\frac{\epsilon_{\rm mech}}{\alpha_{\rm vis}\sin\alpha\,\cos\beta}\frac{v_W}{c}. \tag{B22}$$

If we use the standard value, $\alpha_{\rm vis} = 0.01$, our previous guess of $\epsilon_{\rm mech} = 10^{-2}$, and the angle $\alpha = 0.03$, we find that this ratio is $\sim v_W/c \gg 1$. Reducing $\epsilon_{\rm mech}$ by 2 orders of magnitude would make wind-disk and accretion heating more nearly comparable. A more interesting deduction from equation (B22) is that wind-disk heating and accretion heating have approximately the same dependence on the radial coordinate ϖ.

APPENDIX C

COOLING

Our purpose here is to justify the selection of line coolants and to describe how the cooling rates are calculated. The discussion follows the coolants as a function of decreasing altitude and abundance, starting with hydrogen cooling at the top of the atmosphere.

Hydrogen can cool the upper atmosphere by thermal bremsstrahlung, recombination radiation in transitions to levels $n \geq 2$, and Lyα radiation. We use familiar formulae from Spitzer (1978) for the first two processes, which generally constitute no more than 5% of the total cooling rate. We calculate Lyα cooling in the escape probability formalism:

$$\Lambda_{\rm Ly\alpha} = \beta_{21}A_{21}E_{21}x_2 n_{\rm H}, \tag{C1}$$

$$\beta_{21} = \frac{1-\exp(-\tau_{21})}{\tau_{21}}, \tag{C2}$$

$$\tau_{21} = x_1 N_{\rm H} f_{12}\frac{\pi e^2}{mc}\frac{\lambda_{21}}{\Delta v}, \tag{C3}$$

$$\Delta v = \left[2\pi\left(\sigma_{\rm therm}^2 + \sigma_{\rm turb}^2\right)\right]^{1/2}, \tag{C4}$$

where $\sigma_{\rm therm}$ and $\sigma_{\rm turb}$ are the variances of the thermal and turbulent velocity distributions, respectively. The integer subscripts refer to the two lowest levels of atomic hydrogen, $n = 1$, 2, and the symbols x_1 and x_2 denote the normalized (fractional) populations of these levels. We further assume that the density of atoms in the $n = 2$ level is given by the thermal equilibrium (Boltzmann) formula. The column density in equation (C3) is the (upward) vertical column density $N_\perp$. Figure 3 shows that escaping Lyα radiation is the most important coolant at high temperatures. For the calculations in this paper, we used the value $\sigma_{\rm turb} = 2$ km s^{-1} suggested by observations of the overtone rovibrational transitions of CO (e.g., Najita et al. 1996).

We have also estimated the cooling by molecular hydrogen using the study by Le Bourlot et al. (1999). In both the hot low-$x(H_2)$ and the cool fully associated regimes, cooling by H_2 is at least 4 orders of magnitude smaller than the total and thus negligible. We can extend these results and also rule out any meaningful contribution from other homonuclear molecules like O_2 and N_2.

Heavy atomic ions are potentially important for the temperature range of interest. We start with oxygen, the most abundant element after H and He, and focus on O I, the dominant ion. The densities in the disk atmosphere are higher than the critical densities of both the forbidden optical and the fine-structure far-infrared transitions of O I, so the level populations are close to thermal equilibrium. The forbidden lines are more important in the hot upper layers because both the transition energies and A-values are between 1 and 2 orders of magnitude larger than those of the fine-structure transitions. Their optical depths are also small, whereas the fine-structure lines become thick once $N_\perp > 10^{21}$–10^{22} cm^{-2}. In practice, we have approximated the forbidden-line cooling by an equivalent two-level model, with a level separation of 22,500 K and $A = 8.45\times10^{-3}$ s^{-1}, that allows for subthermal excitation but assumes that the lines are optically thin. The fine-structure cooling due to the $J = 1$–2 (63 μm) and $J = 0$–1 (145 μm) transitions is calculated assuming thermal equilibrium populations but allowing for trapping using appropriate escape probabilities in much the same way as done for Lyα. Before all of the O is transformed into O_2 and H_2O, O I fine structure contributes no more than a few percent of the total cooling in the cool, midaltitude region of the atmosphere where dust cooling dominates.

Based on their spectroscopic properties, the forbidden lines of C II, C I, and N I are expected to make relatively minor contributions to the cooling compared to O I. We also ignore the forbidden and fine-structure lines of heavier ions because of abundance considerations, especially the depletion of refractory elements like Si, Mg, and Fe.

Among the molecular coolants, CO has the greatest potential to affect the gas temperature at intermediate and high altitudes. The pure rotational transitions are relevant for the cooler regions and the rotation-vibrational transitions in the hotter ones. The remainder of this appendix describes how we treat cooling by the rotation-vibrational and pure rotational transitions of CO.

Atomic hydrogen dominates the excitation of the rotation-vibrational transitions of CO if $x_e < 0.01$ and $x(\mathrm{H_2}) < 0.01$ (e.g., Appendix B of Najita et al. 1996; Ayres & Wiedemann 1989), conditions that are well met in the upper atmosphere. Since the density there is smaller than the critical density ($\simeq 10^{11}$ cm^{-3}), the cooling is given by the low-density formula,

$$\Lambda_{\mathrm{CO\ rovib}} = \sum_{Jv,v'J'} n(\mathrm{H}) n_{\mathrm{CO}}(vJ) k(vJ,\ v'J') E(vJ,\ v'J'), \tag{C5}$$

where initial states are labeled vJ and excited states $v'J'$, and $n_{\mathrm{CO}}(vJ)$ is the density of CO in an initial state. Under the conditions in the upper disk atmosphere, the rotational levels of the ground vibrational state are in thermal equilibrium, but the higher vibrational levels (and their rotational distributions) are not. Thus, most of the hot CO in the atmosphere will be in the $v = 0$ level. Using the Boltzmann distribution for its population of rotational levels, equation (C5) can be approximated by

$$\Lambda_{\mathrm{CO\ rovib}} \simeq \sum_{v'} k(0,\ v') E(0,\ v') n_{\mathrm{CO}}(v') n(\mathrm{H}), \tag{C6}$$

where $k(0,\ v')$ is the total H + CO collisional rate coefficient for exciting the vibrational level v and $E(0,\ v')$ is the corresponding excitation energy. The optical depths of the emitted lines are small, and we can obtain a good estimate of the rotation-vibrational cooling by retaining the first two terms of this equation and approximating the vibrational levels by an oscillator spectrum with energy level separation $k_{\mathrm{B}}\theta$ with $\theta = 3084$ K:

$$\Lambda_{\mathrm{CO\ rovib}} \simeq k_{\mathrm{B}}\theta k(1\text{–}0) \frac{e^{-\theta/T}}{1 - e^{-\theta/T}} n(\mathrm{CO}) n(\mathrm{H}) \left[1 + 2\frac{k(2\text{–}0)}{k(1\text{–}0)} e^{-\theta/T} + \cdots\right]. \tag{C7}$$

In converting excitation to de-excitation rates using detailed balance, we have assumed that high-J transitions are involved so that the ratio of statistical weights is essentially unity. We have used the fit by Ayres & Wiedemann (1989) for the $v = 1\text{–}0$ de-excitation rate based on the measurements of Glass & Kironde (1983),

$$k(1\text{–}0) = 7.88 \times 10^{-13} T^{0.5} e^{-1208/T}\ \mathrm{cm^3\ s^{-1}}. \tag{C8}$$

This is close to the one used by Najita et al. (1996) and roughly a factor of 2 smaller than the recent theoretical calculations of Balakrishnan et al. (2002). The ratio $k(2\text{–}0)/k(1\text{–}0)$ is between 0.2 and 0.4, depending on whether one uses experimental (Wight & Leone 1983; McBane et al. 1991) or theoretical information (Balakrishnan et al. 2002). The contributions of higher vibrational levels decrease rapidly beyond $v = 2$ because of decreasing rate coefficients and increasing energy thresholds.

The pure rotational cooling of CO can be calculated assuming that the levels are thermalized. For $T_g > 125$ K, many rotational levels are excited, and two values of J are relevant: $J_m = 8.5(T_2)^{1/2}$ for the peak emission and J_c where thermalization breaks down. Since $J_m \ll J_c$, the cooling can be calculated as

$$\Lambda_{\mathrm{CO\ rot}} = n(\mathrm{CO}) \sum_{1}^{\infty} P_J E_{J,J-1} \beta_{J,J-1} A_{J,J-1}, \tag{C9}$$

where P_J is the Boltzmann distribution for the rotational levels with energies E_J. The symbols $E_{J,J-1} = E_J - E_{J-1}$, $A_{J,J-1}$, and $\beta_{J,J-1}$ stand for the energy change, A-value, and escape probability in the transition $J \rightarrow J - 1$, respectively. Optically thin CO cooling has been discussed by McKee et al. (1982); in the rigid-rotor approximation equation (C9) is

$$\Lambda_{\mathrm{CO\ rot}} = 6 A_{1,0} k_{\mathrm{B}} T_g^2 n(\mathrm{CO}) = 1.86 \times 10^{-23} T_g^2 n(\mathrm{CO})\ \mathrm{ergs\ cm^{-3}\ s^{-1}}. \tag{C10}$$

The utility of this formula is limited by the fact that the lines easily become thick, as can be deduced from the general formula

$$\tau(J-1,\ J) = \frac{3N(\mathrm{CO})}{8\pi\Delta v} \frac{1}{2J-1} P_{J-1} \left(1 - \frac{P_J}{P_{J-1}}\right) A_{1,0} \lambda_{1,0}^{-3}. \tag{C11}$$

At the peak of the emission at J_m,

$$\tau(J_{m-1},\ J_m) \simeq 0.874 \frac{N(\mathrm{CO})_{15}}{\Delta v_5 T_{100}}, \tag{C12}$$

measuring CO column density in units of 10^{15} cm^{-2}, velocity width in km s^{-1}, and T_g in 100 K. When the lines are very optically thick, i.e., when $\tau(J_{m-1},\ J_m) \gg 1$ and $\beta_{J,J-1} \simeq 1/\tau(J-1,\ J)$, equation (C9) can be evaluated exactly as

$$\Lambda_{\mathrm{CO\ rot}} = \frac{n(\mathrm{CO})\Delta v}{N(\mathrm{CO})} \frac{\pi^5}{15} k_{\mathrm{B}} B \left(\frac{T}{B}\right)^5 \lambda_{1,0}^{-3}. \tag{C13}$$

This result is essentially the same as the formula derived by Goldreich & Kwan (1974) for a collapsing spherical cloud, except for geometrical factors. Finally, we adopt the following prescription for CO pure rotational cooling. When $\tau(J_{m-1},\ J_m) < 1$, we use the optically thin formula, equation (C10), and when $\tau(J_{m-1},\ J_m) > 1$, we use the optically thick formula, equation (C13). In practice, CO cooling only plays a significant role in the temperature transition zone, and there it is rovibrational cooling that counts. In this region, CO rotational cooling is well represented by the optically thin limit; when it is thick, it is unimportant in this problem.

Having described how the coolants are calculated, it is appropriate to summarize their effects in qualitative terms. As discussed in § 4, however, it is important to remember that the role of an individual coolant is determined by the heating and the chemistry operative where it is located. Referring to Figures 2 and 3, we see that the thermal structure of the atmosphere can be approximately described in terms of three thermal regimes that are located at different heights above the midplane, each controlled by just one or two coolants in our model, e.g., for $\alpha_h = 0.1$–1.0 at $r = 1$ AU, these layers and their dominant coolants are as follows:

1. *Hot layer.*—$T \geq 2000$–5000 K, $N_\perp < 5\times10^{20}$ cm^{-2}: Lyα and dust cooling.
2. *Warm transition region.*—300 K $< T <$ 2000 K, $N_\perp \simeq 3\times10^{20}$ to 5×10^{21} cm^{-2}: dust cooling and CO rotation-vibrational cooling.
3. *Cool midplane region.*—$T <$ 300 K, $N_\perp > (1$–$5)\times10^{21}$ cm^{-2}: dust cooling.

Cooling of the gas by the dust plays a role in all three thermal regions, starting at the bottom of the hot region. It is also important for answering the question posed in § 1 as to where the dust eventually enforces the gas to be thermally coupled to the dust. From Figure 1 we see that this depends on the strength of the heating; it also depends on the exact coupling criterion. For example, if we require T_g to be no more than 25% larger than T_d, this criterion is not met for the case $\alpha = 1$ until $N_\perp > 10^{22}$ cm^{-2}, where the density $n_{\rm H} > 10^{11}$ cm^{-3}. This is a quite high density, but still several orders of magnitude smaller than the critical density defined in equation (1) for the dust to be decoupled from the gas.

REFERENCES

Aikawa, Y., & Herbst, E. 1999, A&A, 351, 233
Alencar, S. H. P., & Batalha, C. 2002, ApJ, 571, 378
Ardila, D., Basri, G., Walter, F. M., Valenti, J. A., & Johns-Krull, C. M. 2002, ApJ, 566, 1100
Artymowicz, P., & Lubow, S. 1996, ApJ, 467, L77
Ayres, T. R., & Wiedemann, G. R. 1989, ApJ, 338, 1033
Balakrishnan, N., Yan, M., & Dalgarno, A. 2002, ApJ, 568, 443
Balbus, S., & Hawley, J. F. 1991, ApJ, 376, 214
Bergin, E., Calvet, N., D'Alessio, P., & Herczeg, G. J. 2003, ApJ, 591, L159
Bodenheimer, P., & Lin, D. N. C. 2002, Annu. Rev. Earth Planet. Sci., 30, 113
Burke, J. R., & Hollenbach, D. J. 1983, ApJ, 265, 223
Calvet, N., D'Alessio, P., Hartmann, L., Wilner, D., Walsh, A., & Sitko, M. 2002, ApJ, 568, 1008
Calvet, N., Patiño, A., Magris, G. C., & D'Alessio, P. 1991, ApJ, 380, 617
Carr, J. S., Mathieu, R. D., & Najita, J. 2001, ApJ, 551, 454
Carr, J. S., Tokunaga, A. T., & Najita, J. 2004, ApJ, 603, 213
Carr, J. S., Tokunaga, A. D., Najita, J., Shu, F. H., & Glassgold, A. E. 1993, ApJ, 411, L37
Chiang, E. I., & Goldreich, P. 1997, ApJ, 490, 368
D'Alessio, P., Calvet, N., & Hartmann, L. 2001, ApJ, 553, 321
D'Alessio, P., Calvet, N., Hartmann, L., Lizano, S., & Cantó, J. 1999, ApJ, 527, 893
D'Alessio, P., Calvet, N., & Lizano, S. 1998, ApJ, 500, 411
Dalgarno, A., Yan, M., & Liu, W.-H. 1999, ApJS, 125, 237
D'Angelo, G., Henning, T., & Kley, W. 2003, ApJ, 599, 548
Dullemond, C. P., van Zadelhoff, G. J., & Natta, A. 2002, A&A, 389, 464
Elmegreen, B. 1978, Moon Planets, 19, 261
Federman, S. R., Glassgold, A. E., & Kwan, J. 1979, ApJ, 227, 466
Feigelson, E. D., & Montmerle, T. 1999, ARA&A, 37, 363
Feigelson, E. D., et al. 2002, ApJ, 574, 258
Fromang, S., Terquem, C., & Balbus, S. A. 2002, MNRAS, 329, 18
Gammie, C. F. 1996, ApJ, 457, 355
Garmire, G., et al. 2000, AJ, 120, 1426
Glass, G. P., & Kironde, S. 1983, J. Chem. Phys., 86, 908
Glassgold, A. E., Mamon, G. A., & Huggins, P. J. 1991, ApJ, 373, 254
Glassgold, A. E., & Najita, J. 2001, in ASP Conf. Ser. 244, Young Stars near Earth: Progress and Prospects, ed. R. Jayawardhana & T. P. Greene (San Francisco: ASP), 251
Glassgold, A. E., Najita, J., & Igea, J. 1997, ApJ, 480, 344 (erratum 485, 820) (G97)
Goldreich, P., & Kwan, J. 1974, ApJ, 189, 441
Goldreich, P., & Ward, W. R. 1973, ApJ, 183, 1051
Gorti, U., & Hollenbach, D. J. 2004, ApJ, 613, 642
Hartmann, L., & Kenyon, S. J. 1987a, ApJ, 312, 243
———. 1987b, ApJ, 322, 393
Herczeg, G. J., Linsky, J. L., Valenti, J. A., Johns-Krull, C. M., & Wood, B. E. 2002, ApJ, 572, 310
Herczeg, G. J., Wood, B. E., Linsky, J. L., Valenti, J., & Johns-Krull, C. M. 2004, ApJ, 607, 369
Hollenbach, D. J., & McKee, C. F. 1979, ApJS, 41, 555
Hollenbach, D. J., & Salpeter, E. E. 1971, ApJ, 163, 155
Hollenbach, D. J., Yorke, H. W., & Johnstone, D. 2000, in Protostars and Planets IV, ed. V. Mannings, A. P. Boss, & S. Russell (Tucson: Univ. Arizona Press), 401
Igea, J., & Glassgold, A. E. 1999, ApJ, 518, 848 (IG99)
Ilgner, M., Henning, Th., Markwick, A. J., & Millar, T. J. 2004, A&A, 415, 643
Kamp, I., van Zadelhoff, G.-H., van Dishoeck, E., & Stark, R. 2003, A&A, 397, 1129
Kastner, J. H., & Weintraub, D. A. 2002, ApJ, 567, 434
Kim, S.-H., Martin, P. G., & Hendry, P. D. 1994, ApJ, 422, 164
Klahr, H. H., & Bodenheimer, P. 2003, ApJ, 582, 869
Kominami, J., & Ida, S. 2002, Icarus, 157, 43
Le Bourlot, J., Pineau des Forêts, G., & Flower, D. R. 1999, MNRAS, 305, 802
Lubow, S. H., & Ogilvie, G. I. 1998, ApJ, 504, 983
Mathis, J. S., Rumpl, W., & Nordsieck, K. H. 1977, ApJ, 217, 425
McBane, G. C., Kable, S. H., Houston, P. L., & Schatz, G. C. 1991, J. Chem. Phys., 94, 1141
McCabe, C., Duchêne, G., & Ghez, A. M. 2003, ApJ, 588, L113
McKee, C. F., Storey, J. W. V., Watson, D. M., & Green, S. 1982, ApJ, 259, 647
Miller, K. A., & Stone, J. M., 2000, ApJ, 534, 398
Miyake, K., & Nakagawa, Y. 1993, Icarus, 106, 20
Morrison, R., & McCammon, D. 1983, ApJ, 270, 119
Muzerolle, J., et al. 2000, ApJ, 535, L47
Najita, J. 2004, in ASP Conf. Ser., Star Formation in the Interstellar Medium, ed. D. Johnstone, F. C. Adams, D. N. C. Lin, D. A. Neufeld, & E. C. Ostriker (San Francisco: ASP), in press
Najita, J., Carr, J. S., Glassgold, A. E., Shu, F. H., & Tokunaga, A. T. 1996, ApJ, 462, 919
Najita, J., Carr, J. S., & Mathieu, R. D. 2003, ApJ, 589, 931
Najita, J., Edwards, S., Basri, G., & Carr, J. 2000, in Protostars and Planets IV, ed. V. Mannings, A. P. Boss, & S. S. Russell (Tucson: Univ. Arizona Press), 457
Najita, J., & Shu, F. H. 1994, ApJ, 429, 808
Ogilvie, G. I., & Lubow, S. H. 1999, ApJ, 515, 767
Pringle, J. 1981, ARA&A, 19, 137
Shang, H., Glassgold, A. E., Shu, F. H., & Lizano, S. 2002, ApJ, 564, 853
Shu, F. H., Najita, J., Ostriker, E. C., & Shang, H. 1995, ApJ, 455, L155
Shull, M., & van Steenberg, M. E. 1985, ApJ, 298, 268
Spitzer, L., Jr. 1949, ApJ, 109, 337
———. 1978, Diffuse Matter in Space (New York: Wiley)
Spitzer, L., Jr., & Jenkins, E. 1975, ARA&A, 13, 133
Stone, J. M., Gammie, C. F., Balbus, S. A., & Hawley, J. F. 2000, in Protostars and Planets IV, ed. V. Mannings, A. P. Boss, & S. S. Russell (Tucson: Univ. Arizona Press), 589

Takahashi, T., Silk, J., & Hollenbach, D. J. 1983, ApJ, 275, 145
Valenti, J. A., Johns-Krull, C. M., & Linsky, J. L. 2000, ApJS, 129, 399
Weidenschilling, S. J. 1997, Icarus, 127, 290
Weidenschilling, S. J., & Cuzzi, J. N. 1993, in Protostars and Planets III, ed. M. S. Mathews (Tucson: Univ. Arizona Press), 1031
Wight, C. A., & Leone, S. R. 1983, J. Chem. Phys., 78, 4875
Willacy, K., & Langer, W. D. 2000, ApJ, 544, 903
Wolf, S. 2003, ApJ, 582, 859
Wolf, S., Padgett, D., & Stapelfeldt, K. 2003, ApJ, 588, 373
Wood, K., et al. 2001, ApJ, 561, 299